Modified Tacrine Derivatives as Multitarget-Directed Ligands for the Treatment of Alzheimer's Disease: Synthesis, Biological Evaluation, and Molecular Modeling Study

Salma Fares, Walaa M. El Husseiny,* Khalid B. Selim, and Mohammed A. M. Massoud

Read Online

ACCESS | Metrics & More | Article Recommendations | SI Supporting Information

ABSTRACT: To develop multitarget-directed ligands (MTDLs) as potential treatments for Alzheimer's disease (AD) and to shed light on the effect of the chromene group in designing these ligands, 35 new tacrine-chromene derivatives were designed, synthesized, and biologically evaluated. Compounds **5c** and **5d** exhibited the most desirable multiple functions for AD; they were strong $hAChE$ inhibitors with IC_{50} values of 0.44 and 0.25 μM, respectively. Besides, their potent BuChE inhibitory activity was 10- and 5-fold more active than rivastigmine with IC_{50} = 0.08 and 0.14 μM, respectively. Moreover, they could bind to the peripheral anionic site (PAS), influencing Aβ aggregation and decreasing Aβ-related neurodegeneration, especially compound **5d**, which was 8 times more effective than curcumin with IC_{50} = 0.74 μM and 76% inhibition at 10 μM. Compounds **5c** and **5d** showed strong BACE-1 inhibition at the submicromolar level with IC_{50} = 0.38 and 0.44 μM, respectively, which almost doubled the activity of curcumin. They also showed single-digit micromolar inhibitory activity against MAO-B with IC_{50} = 5.15 and 2.42 μM, respectively. They also had antioxidant activities and showed satisfactory metal-chelating properties toward Fe^{+2}, Zn^{+2}, and Cu^{+2}, inhibiting oxidative stress in AD brains. Furthermore, compounds **5c** and **5d** showed acceptable relative safety upon normal cells SH-SY5Y and HepG2. It was shown that **5c** and **5d** were blood−brain barrier (BBB) penetrants by online prediction. Taken together, these multifunctional properties highlight that compounds **5c** and **5d** can serve as promising candidates for the further development of multifunctional drugs against AD.
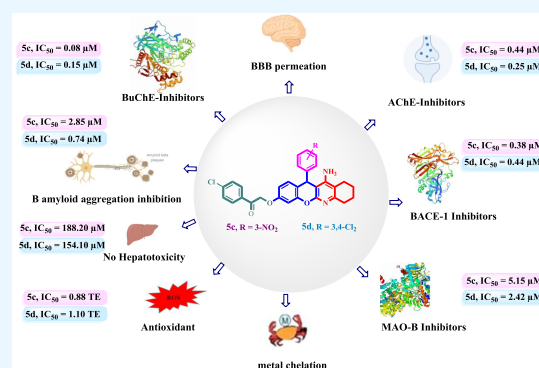
1. INTRODUCTION

Alzheimer's disease (AD) is a progressive, chronic, fatal, and devastating neurological disease affecting mainly the elderly. AD is characterized by cognitive impairments, including progressive memory loss, a decline in language skills, disorientation, and behavioral disturbances, eventually causing incapacitation and death.[1,2]

Several hypotheses have been proposed to explain the etiology of AD, which includes a decrease of the neurotransmitter acetylcholine (ACh),[3,4] accumulation of insoluble forms of amyloid-β (Aβ) and hyperphosphorylated tau protein,[5] oxidative stress,[6] neuroinflammation of the central nervous system,[7] metabolic homeostasis disruption of metals,[8] and β secretase-1 (BACE-1) activation.[9] Thus, the conventional paradigm of "one drug, one target" may not be suitable enough to treat this complicated disease. To address this issue, a multitarget-directed ligand (MTDL) strategy means that one molecule can simultaneously act on multitargets related to the disease, which has been put forward as a potential approach for the treatment of AD.[10]

Currently, the main approved AD therapy has been focused on increasing cholinergic transmission *via* the accumulation of ACh in the neuronal synaptic cleft, by inhibiting acetylcholi-nesterase (AChE).[11,12] At present, with the exception of memantine, all FDA-approved drugs such as donepezil, rivastigmine, and galantamine are AChE inhibitors (AChEIs).[13] The crystal structure of AChE shows that it consists of two binding sites: one is a catalytic anionic site (CAS) and the other is a peripheral anionic site (PAS), which are connected by a 20 Å deep gorge.[14] Generally, inhibitors binding to either one site can inhibit AChE. Thus, AChE inhibitors, like donepezil, that can simultaneously act on CAS and PAS appear to be more beneficial for AD treatment.[15] However, recent studies indicate that AChE also plays a role in inducing the aggregation of Aβ through the interaction of PAS with Aβ peptides.[11,12] AChEIs are expected not only to relieve the symptoms but also to reduce the progression of AD.[16,17] Besides AChE, butyrylcholinesterase (BuChE) is another target of interest in the search for anti-Alzheimer drugs, as
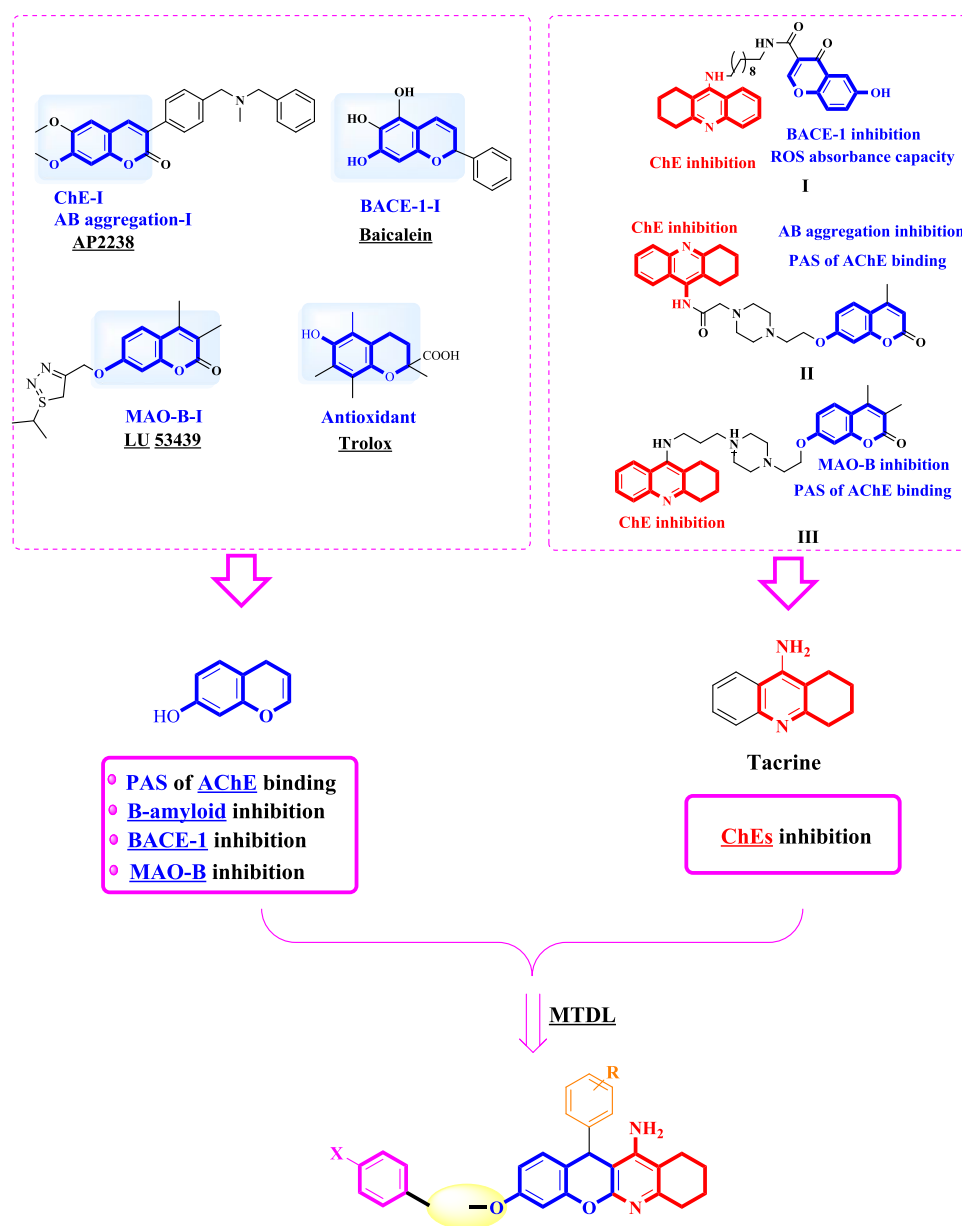
Figure 1. Design strategy for the synthesis of modified tacrine-chromene derivatives.

this enzyme exerts a compensatory effect in response to a greatly decreased AChE activity in the central nervous system (CNS).[18]

The pathophysiology of AD is complex, and the main histopathological hallmarks of AD are the presence of extracellular senile plaques (SPs) caused by the deposits of Aβ peptide and intracellular neurofibrillary tangles (NFTs) formed by abnormally phosphorylated tau.[19] Aβ is generated through proteolytic cleavage of the β-amyloid precursor protein (APP) by β- and γ-secretase activities.[20] Aβ accumulation is proposed to be an early, potentially initiating, event in the pathogenesis of AD like dementia, and neuron death.[21,22] Meanwhile, transition metals such as copper, iron, and zinc ions were postulated to bind Aβ peptides, leading to neurotoxicity and oxidative stress accompanied by β-deposition.[23−25] Hence, metal chelation, BACE-1, and Aβ have become well-established targets for AD treatment by inhibiting Aβ aggregation *via* the modulation or inhibition of

enzymes accountable for Aβ aggregation (BACE-1 and γ-secretase).[26,27]

Also, monoamine oxidase (MAO) is an efficient therapy target in the treatment of AD. MAO-B is responsible for the oxidative deamination of various biogenic and xenobiotic amines.[28] Accumulated evidence shows that the MAO-B activity increases with age, especially in AD patients, and a significant activity rise is found in the brain tissue, cerebral spinal fluid (CSF), as well as in platelets.[29] The elevated activity of MAO-B leads to an enhanced metabolism of dopamine and an increased level of hydrogen peroxide and oxidative free radicals, which give rise to neuronal damage.[30,31] Furthermore, the activated MAO-B can also cause disorder of the cholinergic system, destroy cholinergic neurons, and promote the formation of amyloid plaques.[32] Thus, inhibition of MAO-B may provide another potential approach for treating AD. For example, selegiline and rasagiline, as MAO-B inhibitors, have been shown to significantly improve learning
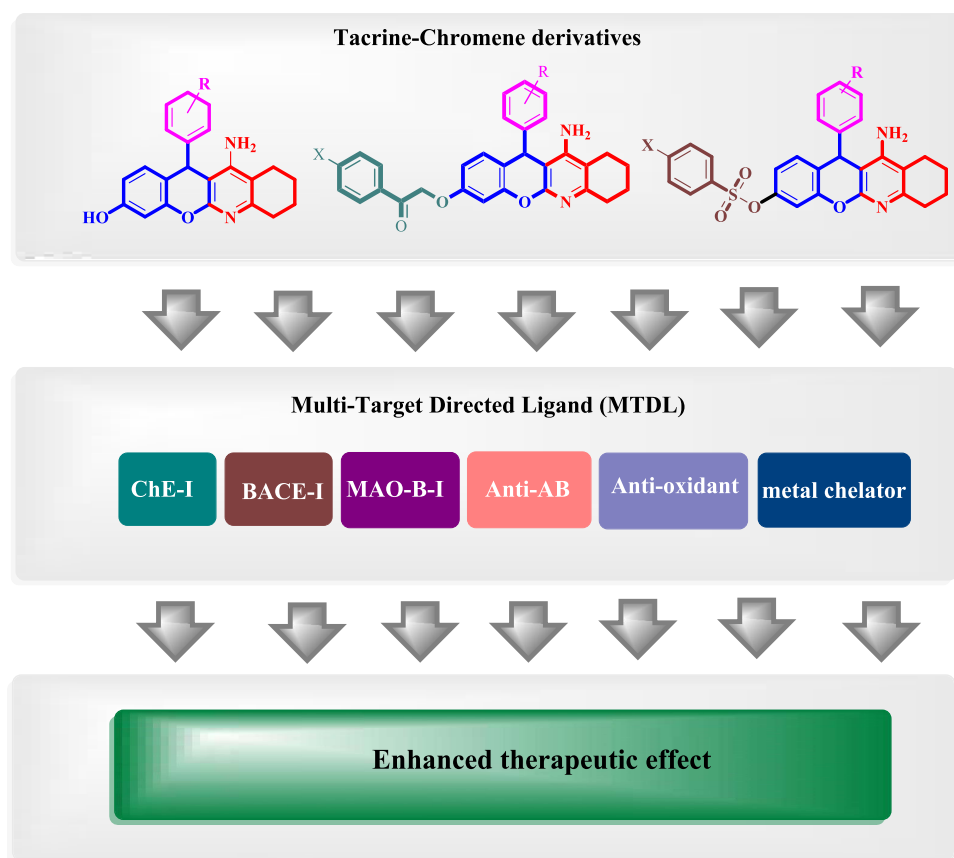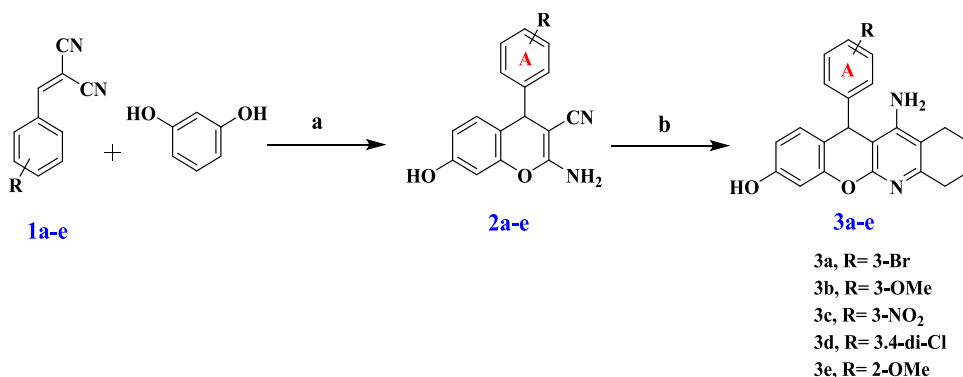
Figure 2. Multitarget-directed ligand (MTDL) of modified tacrine-chromene derivatives.

Scheme 1. Synthetic Route for the Preparation of Modified Tacrine Derivatives 3a–e[a]

3a, R= 3-Br
3b, R= 3-OMe
3c, R= 3-NO$_2$
3d, R= 3.4-di-Cl
3e, R= 2-OMe

[a]Reagents and condition: (a) EtOH, piperidine, reflux 24 h; (b) AlCl$_3$, 1,2-dichloroethane (DCE), cyclohexanone, reflux 3–5 h.

and memory deficits in animal models associated with AD and to slow the disease progression in AD patients.[33,34]
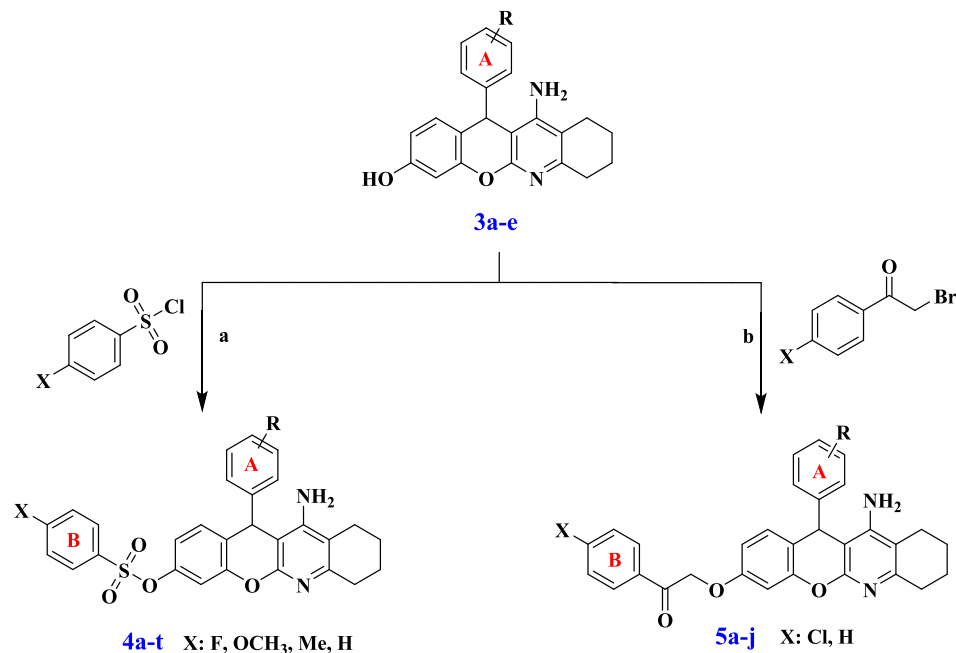
Tacrine, an amino acridine derivative, was the first AChE inhibitor approved for treatment of AD,[14] and it was withdrawn from the market due to its hepatotoxicity.[35] To solve this problem, replacement of the benzene ring in the tacrine structure was developed using different heterocyclic systems in order to obtain new derivatives with high anticholinesterase and selective peripheral binding potency.[36,37]

Chromenes, which are present in many natural and synthetic compounds, have exhibited potent biological activities related to neurological disorders (Figure 1).[38,39] For example, AP2238 can interact with the PAS of AChE and serve as one part of the dual binding mode of action; also, it exerts an Aβ preaggregation inhibitory action mediated by its peripheral binding site.[40]

Moreover, baicalein[41] and LU 53439[42] were found to treat neurodegenerative diseases through their BACE-1 and MAO-B inhibitory activities, respectively. The last example is Trolox, a water-soluble analogue of vitamin E, which prevents apoptosis due to its antioxidant activity.[43]

Given the activities of tacrine and chromene, a series of multitarget compounds possessing tacrine-chromene derivatives have been designed and synthesized recently (Figure 1). The tacrine part was responsible for ChE inhibition, whereas chromene counterparts were responsible for the inhibition of

Scheme 2. Synthetic Route for the Preparation of Modified Tacrine Derivatives 4a−t and 5a−j[a]

Comp.	R	X	Comp.	R	X	Comp.	R	X
4a	3-Br		4k	3-Br		5a	3-Br	
4b	3-OMe		4l	3-OMe		5b	3-OMe	
4c	3-NO$_2$	F	4m	3-NO$_2$	Me	5c	3-NO$_2$	Cl
4d	3,4-Cl$_2$		4n	3,4-Cl$_2$		5d	3,4-Cl$_2$	
4e	2-OMe		4o	2-OMe		5e	2-OMe	
4f	3-Br		4p	3-Br		5f	3-Br	
4g	3-OMe		4q	3-OMe		5g	3-OMe	
4h	3-NO$_2$	OMe	4r	3-NO$_2$	H	5h	3-NO$_2$	H
4i	3,4-Cl$_2$		4s	3,4-Cl$_2$		5i	3,4-Cl$_2$	
4j	2-OMe		4t	2-OMe		5j	2-OMe	

[a]Reagents and condition: (a) K$_2$CO$_3$, acetone, reflux, 3−5 h; (b) K$_2$CO$_3$, acetone, reflux, 3−5 h.

BACE-1,[44] Aβ aggregation,[45] and MAO-B[46] as revealed in compounds I,[44] II,[45] and III.[46]

In an attempt to obtain new multitarget molecules with AChE, BACE-1, Aβ, and MAO-B inhibitory activities for AD treatment, a series of novel compounds have been designed and synthesized by replacement of the benzene ring of tacrine with chromene to produce modified tacrine-chromene hybrids. Tacrine was chosen to inhibit the ChE, and the chromene scaffold was used for BACE-1 and MAO-B inhibition. Besides, due to the aromatic character of the tacrine-chromene, it might have potential interaction with the PAS of AChE and have Aβ aggregation inhibition activity (Figure 2).

2. RESULTS AND DISCUSSION

2.1. Chemistry. Novel modified tacrine derivatives 3a−e, 4a−t, and 5a−j were synthesized as described in Schemes 1 and 2. The key starting compounds, 2-arylidene malononitriles[47] 1a−e, were prepared via the Knoevenagel condensation of malononitrile with different aromatic aldehydes. Compounds 1a−e reacted with resorcinol to give 2-amino-7-hydroxy-4-substituted-chromene-3-carbonitriles 2a−e through Michael addition.[48] The Friedländer reaction[49] of 2a−e with

cyclohexanone in the presence of AlCl$_3$ gives the target compounds 3a−e in excellent yields (Scheme 1).

As shown in Scheme 2, treating 3a−e with the appropriate aryl sulfonyl chloride derivatives in a basic medium afforded the modified tacrine-chromeno-sulfonate derivatives 4a−t.[50,51] On the other hand, reaction of 3a−e with bromoacetophenone derivatives generated the modified tacrine-chromeno-aceto-phenone derivatives 5a−j.[52]

The infrared (IR) spectra of all synthesized compounds 3a−e, 4a−t, and 5a−j showed two sharp peaks for NH$_2$ groups in the region 3227−3502 cm^{-1}. Broad bands of OH groups were observed in the region 3093−3450 cm^{-1} for compounds 3a−e but vanished for compounds 4a−t and 5a−j. Compounds 4a−t demonstrated sulfonyl peaks at 1350−1380 cm^{-1}, while compounds 5a−j revealed sharp peaks for the ketone carbonyl groups in the region 1695−1721 cm^{-1}.

The ^{1}H NMR spectra of compounds 3a−e, 4a−t, and 5a−j showed C−H protons of cyclohexene rings between 1.69 and 2.99 ppm as singlet and multiplet peaks. Also, the C−H proton of the pyran ring was observed as a singlet peak between 5.19 and 5.67 ppm. In addition, D$_2$O exchangeable NH$_2$ of compounds 3a−e, 4a−t, and 5a−j appeared as a singlet peak

in the regions δ 5.28 and 5.84 ppm. Signals of the D_2O exchangeable OH group for compounds **3a−e** appeared as a singlet peak between 9.52 and 9.66 ppm and vanished in compounds **4a−t** and **5a−j**. Signals of $COCH_2O$ protons in compounds **5a−j** were detected between 5.57 and 5.61 ppm as a singlet peak.

The ^{13}C NMR spectra of compounds **3a−e**, **4a−t**, and **5a−j** showed $-CH_2$ of cyclohexene rings between 21.24 and 33.09 ppm. Also, the $-CH$ of the pyran ring was observed between 33.11 and 38.87 ppm. Compounds **5a−e** showed ketonic carbonyl peaks at 192.92−194.97 ppm and particular peaks at 70.65−70.77 for the methylene group $COCH_2O$.

2.2. Biological Screening. *2.2.1. Inhibitory Activity against hAChE.* AChE is the enzyme responsible for the hydrolysis of ACh, thus terminating its effect on the cholinergic receptors. Accordingly, its inhibition would be expected to increase the amount of ACh to be available for neuronal transmission at the receptor site, which is expected to be successful in relieving some cognitive and behavioral symptoms of AD.[53] All of the synthesized compounds were evaluated *in vitro* to measure their inhibitory effect (IC_{50}, μM) against AChE *via* the Ellman method[54] using tacrine, donepezil, and rivastigmine as standards for comparison as well as to measure the effect of the nature of the substituents on rings A and B. As shown in Table 1, modified tacrine-chromenol compounds (**3a−e**) exhibited IC_{50} in the range of 3.48−26.65 μM. Compound **3a** with an electronegative bromo atom at the 3-position of ring A showed an elevation of the AChE inhibitory activity with IC_{50} 3.48 μM in comparison to compounds **3b** (3-OMe) and **3c** (3-NO_2), which showed the least activities, while compounds **3d** (3,4-Cl_2) and **3e** (2-OMe) showed inhibitory activities with IC_{50} = 5.31 and 5.88 μM, respectively.

Introduction of aryl sulfonates to compounds **3a−e** gave compounds **4a−t**. Generally, as shown in Table 1 and Figure 3, the AChE inhibition profile of tacrine-chromeno-aryl sulfonate conjugates increases in the presence of electron-donating substituents (3-OMe and 3-Me) and decreases in the presence of an electronegative substituent (3-F) on ring B. It was revealed that compounds **4f−j** with an electron-donating methoxy group exhibited the highest AChE inhibitory activity with IC_{50} in the range of 0.30−5.16 μM. Compound **4g**, which possesses a 3-methoxy substituent on ring A and ring B, showed the strongest AChE inhibitory activity at the submicromolar level (IC_{50} = 0.30 μM). However, the replacement of the 3-methoxy group with a 2-methoxy group in ring A led to a decline in the activity (**4j**, IC_{50} = 5.16 μM). It was well-established that methyl-substituted derivatives **4k−o** on ring B were less potent than the corresponding methoxy-substituted counterparts as they were exhibiting IC_{50} from 0.47 to 11.14 μM, and the best efficacy was related to compound **4n** (3,4-Cl_2 substituent). Moreover, compounds **4a−e** with a 4-fluoro atom on ring B exhibited AChE inhibitory activities with an IC_{50} range of 0.62−22.38 μM, while compounds **4p−t** without substitution on ring B were the least active compounds with IC_{50} ranging from 1.34 to 24 μM. Regarding the substitution on ring A, it had diverse effects, but the results show that compounds **4e**, **4j**, and **4t** with the 2-OMe group have the least AChE inhibitory activity except for compound **4o**, which displayed AChE inhibitory activity with an IC_{50} value of 1.03 μM.

On the other hand, the third series of tacrine-chromeno acetophenone conjugates **5a−j** showed a remarkable increase

Table 1. IC_{50} Values of Compounds 3a−e, 4a−t, and 5a−j against AChE[a]

compd.	R	X	*in vitro* AChE inhibition $IC_{50} \pm SD$ (μM)	BBB permeation (+/−) and BBB score[b]
3a	3-Br		3.48 ± 0.19	BBB + (0.093)
3b	3-OMe		26.65 ± 1.42	BBB + (0.090)
3c	3-NO_2		15.09 ± 0.8	BBB + (0.087)
3d	3,4-Cl_2		5.31 ± 0.28	BBB + (0.081)
3e	2-OMe		5.88 ± 0.31	BBB + (0.076)
4a	3-Br	F	3.88 ± 0.21	BBB + (0.212)
4b	3-OMe	F	13.53 ± 0.72	BBB + (0.172)
4c	3-NO_2	F	0.62 ± 0.03	BBB + (0.163)
4d	3,4-Cl_2	F	6.09 ± 0.32	BBB + (0.153)
4e	2-OMe	F	22.38 ± 1.19	BBB + (0.159)
4f	3-Br	OMe	0.73 ± 0.03	BBB + (0.182)
4g	3-OMe	OMe	0.30 ± 0.01	BBB + (0.176)
4h	3-NO_2	OMe	1.53 ± 0.07	BBB + (0.148)
4i	3,4-Cl_2	OMe	2.20 ± 0.1	BBB + (0.134)
4j	2-OMe	OMe	5.16 ± 0.22	BBB + (0.164)
4k	3-Br	Me	9.35 ± 0.4	BBB + (0.159)
4l	3-OMe	Me	2.62 ± 0.11	BBB + (0.143)
4m	3-NO_2	Me	11.14 ± 0.48	BBB + (0.126)
4n	3,4-Cl_2	Me	0.47 ± 0.02	BBB + (0.111)
4o	2-OMe	Me	1.03 ± 0.04	BBB + (0.130)
4p	3-Br	H	1.34 ± 0.07	BBB + (0.158)
4q	3-OMe	H	2.45 ± 0.12	BBB + (0.151)
4r	3-NO_2	H	5.50 ± 0.28	BBB + (0.151)
4s	3,4-Cl_2	H	9.69 ± 0.49	BBB + (0.138)
4t	2-OMe	H	24 ± 1.21	BBB + (0.145)
5a	3-Br	Cl	0.99 ± 0.05	BBB + (0.082)
5b	3-OMe	Cl	6.01 ± 0.3	BBB + (0.060)
5c	3-NO_2	Cl	0.44 ± 0.02	BBB + (0.079)
5d	3,4-Cl_2	Cl	0.25 ± 0.01	BBB + (0.068)
5e	2-OMe	Cl	0.75 ± 0.04	BBB + (0.046)
5f	3-Br	H	1.14 ± 0.054	BBB + (0.054)
5g	3-OMe	H	31.01 ± 1.47	BBB + (0.031)
5h	3-NO_2	H	10.17 ± 0.48	BBB + (0.052)
5i	3,4-Cl_2	H	0.56 ± 0.03	BBB + (0.068)
5j	2-OMe	H	2.48 ± 0.12	BBB + (0.017)
Tacrine			0.19 ± 0.01	BBB + (0.120)
Rivastigmine			3.58 ± 0.19	BBB + (0.042)
Donepezil			0.13 ± 0.01	BBB + (0.135)

[a]All of the results are reported as $IC_{50} \pm$ standard error of the mean (SEM) (n = 3) for three independent experiments. [b]The BBB permeability was predicted using the online BBB prediction server (http://www.cbligand.org/BBB/).

in activity when compared to the series of tacrine-chromenol compounds **3a−e**. A reverse trend in the AChE inhibitory activity was observed among the third series, and the addition of an electron-withdrawing substituent on ring B led to a sharp increase in the inhibitory activity. Chloro-containing substituents on ring B **5a−e** exhibited a superior inhibitory activity toward AChE than compounds **5f−j** with IC_{50} values of 0.25−6.01 and 0.56−31.01 μM, respectively. Chloroacetophenone derivatives bearing 3,4-Cl_2 (**5d**) were the most effective AChE inhibitors with IC_{50} 0.25 μM. Compounds **5c** (3-NO_2) and **5e** (2-OMe) displayed strong submicromolar AChE inhibitory activity with IC_{50} values of 0.44 and 0.75 μM, respectively. Conversely to tacrine-chromeno aryl sulfonate conjugates, 2-OMe containing compounds on ring A **5e** and **5j** revealed an advanced inhibitory action against AChE with IC_{50} values of
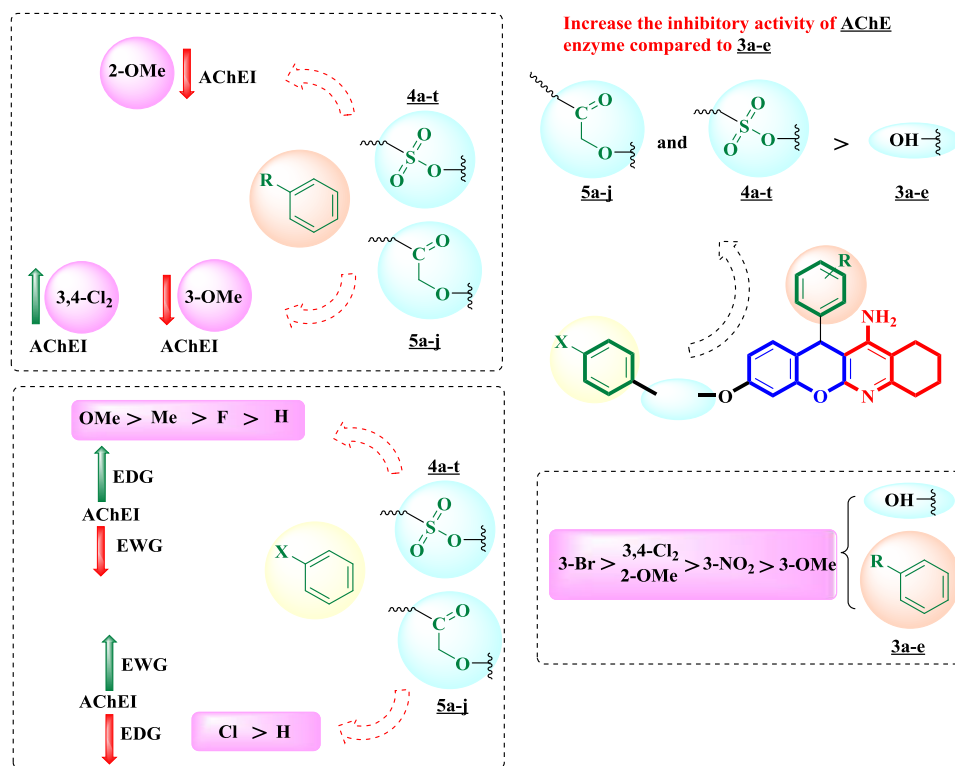
Figure 3. Generalized structure−activity relationship (SAR) of compounds **3a−e**, **4a−t**, and **5a−j** on AChE inhibition.

Table 2. Experimental Results for BuChE, BACE-1, and MAO-B Inhibition Assays[c]

compd. no.	ChE inhibitors IC$_{50}$ ± SD (μM)		SI[a]	SI[b]	IC$_{50}$ ± SD (μM)	
	AChE	BuChE			BACE-1	MAO-B
4c	0.62 ± 0.03	0.69 ± 0.041	1.11	0.90	2.68 ± 0.123	8.04 ± 0.27
4g	0.30 ± 0.01	0.35 ± 0.021	1.18	0.85	1.46 ± 0.068	12.7 ± 0.43
4n	0.47 ± 0.02	0.18 ± 0.011	0.38	2.59	**0.25 ± 0.011**	3.73 ± 0.13
5c	0.44 ± 0.02	**0.08 ± 0.005**	0.19	5.37	0.38 ± 0.017	5.15 ± 0.17
5d	**0.25 ± 0.01**	0.14 ± 0.009	0.59	1.69	0.44 ± 0.021	2.42 ± 0.08
5i	0.56 ± 0.03	0.26 ± 0.016	0.47	2.12	2.12 ± 0.098	**1.62 ± 0.05**
Tacrine	0.19 ± 0.01	0.02 ± 0.002	0.14	7.31	ND	ND
Rivastigmine	3.58 ± 0.19	0.81 ± 0.049	0.22	4.39	ND	ND
Donepezil	0.13 ± 0.01	0.21 ± 0.013	1.61	0.617	3.22 ± 0.2	ND
Curcumin	ND	ND			0.67 ± 0.031	ND
Iproniazid	ND	ND			ND	7.7 ± 0.4
Selegiline	ND	ND			ND	0.64 ± 0.02

[a]AChE SI (selectivity index) = IC$_{50}$ of BuChE/IC$_{50}$ of AChE. [b]BuChE SI (selectivity index) = IC$_{50}$ of AChE/IC$_{50}$ of BuChE. [c]ND, not determined.

0.75 and 2.48 μM, respectively, whereas the inclusion of the electron-donating group 3-OMe led to a sharp decrease in the inhibitory activity as revealed in compounds **5b** (IC$_{50}$ = 6.01 μM) and **5g** (IC$_{50}$ = 31.01 μM). The optimum substituents on ring A used in this aspect were 3,4-Cl$_2$ as compounds **5d** and **5i** had the best AChE-I activity.

Based on the result gathered in Table 1 and Figure 3, compounds **4c**, **4g**, **4n**, **5c**, **5d**, and **5i**, which revealed the highest potencies with submicromolar AChE inhibitory activity with IC$_{50}$ values of 0.62, 0.30, 0.47, 0.44, 0.25, and 0.56 μM, respectively, were selected for further screening against AD.

2.2.2. Inhibitory Activity against hBuChE. The six promising active AChE inhibitors **4c**, **4g**, **4n**, **5c**, **5d**, and **5i** were evaluated by the modified Ellman method[54] using tacrine, donepezil, and rivastigmine (well-known inhibitors for

BuChE) as references drugs. Subsequently, IC$_{50}$ values of the final compounds showing inhibition above 50% were calculated, and the results are reported in Table 2. The results showed that all of the tested compounds showed a remarkable BuChE inhibition in the submicromolar range from 0.08 to 0.69 μM. Chromene-chloroacetophenone conjugates are not only important for AChE inhibition but also critical for BuChE as compounds **5c** and **5d** were the most active compounds. Compound **5c** bearing the Cl-acetophenone part with the 3-NO$_2$ substituent on ring A elicited excellent BuChE inhibition in the two-digit nanomolar range with an IC$_{50}$ value of 0.08 μM, almost 10-fold more active than rivastigmine. Besides, **5d** with 3,4-Cl$_2$ substituents with an IC$_{50}$ value of 0.14 μM was almost 5-fold more active. Compounds **4n** and **5i** (IC$_{50}$ values of 0.18 and 0.26 μM, respectively) were nearly 4-fold more

active, while **4g** and **4c** (IC$_{50}$ values of 0.35 and 0.69 μM, respectively) had almost double the activity of rivastigmine, respectively. The occupancy of meta positions with EWGs on ring A could yield higher AChE and BuChE inhibition as the majority of potent compounds possess 3-NO$_2$ and 3,4-Cl$_2$ substituents.

2.2.3. Inhibitory Activity against β-Secretase. Several independent approaches led to the identification of the β-site amyloid precursor protein cleavage enzyme (BACE-1) as the first enzyme of the amyloid cascade.[55,56] Using the FRET-based BACE-1 fluorescence assay kit, compounds **4c**, **4g**, **4n**, **5c**, **5d**, and **5i** were evaluated for their inhibitory activity against BACE-1 using curcumin and donepezil as reference compounds. The tested compounds were more potent inhibitors against BACE-1 than donepezil, with IC$_{50}$ ranging from 0.25 to 2.68 μM. Compound **4n** (sulfonate derivative) was the most active compound among the tested series with IC$_{50}$ = 0.25 μM, which had almost triple the activity of curcumin. However, compounds **5c** and **5d** (acetophenone derivatives) showed strong inhibition at the submicromolar level with IC$_{50}$ values of 0.38 and 0.44 μM, respectively, which were nearly double the activity of curcumin.

2.2.4. Inhibitory Activity against MAO-B. Selective inhibition of MAO-B provides another therapeutic approach to treat AD. The inhibitory activity against *h*MAO-B was measured for the promising compounds **4c**, **4g**, **4n**, **5c**, **5d**, and **5i** using iproniazid (nonselective MAO inhibitor) and selegiline (selective MAO-B inhibitor) as reference compounds. As shown in Table 2, most of the hybrids showed single-digit micromolar inhibitory activity, effectively inhibiting MAO-B with IC$_{50}$ ranging from 1.62 to 8.04 μM. Only compound **4g** showed two-digit micromolar inhibitory activity with IC$_{50}$ equal to 12.7 μM. Sulfonate derivative **4n** (IC$_{50}$ = 3.37 μM) bearing 3,4-Cl$_2$ substituents on ring A was more active than the other derivatives **4c** and **4g**. Again, acetophenone derivatives showed the best activity; compounds **5i** and **5d** (IC$_{50}$ = 1.62 and 2.42 μM) having 3,4-Cl$_2$ substituents on ring A were more active than compound **5c** (IC$_{50}$ = 5.15 μM) having the 3-NO$_2$ substituent on ring A. The 3,4-Cl$_2$ substituents on ring A afforded the most potent MAO-B inhibitors **4n**, **5d**, and **5i** with inhibitory activities nearly 2, 3, and 4 times better than that of iproniazid (IC$_{50}$ = 7.7 μM), respectively.

2.2.5. Inhibition of Self-Induced Aβ$_{1-42}$ Aggregation. In an AD patient's brain, senile plaques, the abnormal aggregates of amyloid β, are observed as the major hallmarks of this disease.[5] Compounds **4c**, **4g**, **4n**, **5c**, **5d**, and **5i** as potent AChE, BuChE, BACE-1, and MAO-B inhibitors were evaluated for their β amyloid aggregation inhibition ability through the fluorescence method[57] using curcumin (potent antiamyloido-genic agent) as a reference compound.[58] The result indicated that the tested compounds were promising Aβ inhibitors as their Aβ$_{1-42}$ aggregation inhibition ranged from 40 to 76% compared to curcumin's 44%. It was evident that acetophe-none conjugates **5c**, **5d**, and **5i** exhibited stronger inhibitory activity against Aβ (IC$_{50}$ = 2.85, 0.74, and 1.41 μM, respectively) compared to phenyl sulfonate conjugates **4c**, **4g**, and **4n**, (IC$_{50}$ = 4.28, 11.7, and 17.37 μM). Again, acetophenone conjugates with 3,4-Cl$_2$ substituents on ring A showed superior activity. Aβ aggregation was more susceptible to the derivative **5d** than the others as it was the most effective compound (IC$_{50}$ = 0.74, 76% inhibition at 10 μM), which is more active than curcumin (IC$_{50}$ = 6.53, 44%) by 8 times; see Table 3.

Table 3. Inhibition of Aβ Aggregation by Promising Compounds

compd. no.	aggregation inhibition	
	Aβ$_{1-42}$ IC$_{50}$ (μM)	Aβ$_{1-42}$ (% inhibition at 10 μM)
4c	4.28 ± 0.17	47%
4g	11.7 ± 0.45	43%
4n	17.37 ± 0.68	40%
5c	2.85 ± 0.11	59%
5d	**0.74 ± 0.03**	**76%**
5i	1.41 ± 0.05	68%
Curcumin	6.53 ± 0.25	44%

2.2.6. Antioxidant Activity. The elevated production of reactive oxygen species (ROS) is suggested to promote the progression of AD.[59] Therefore, the total antioxidant capacity (TAC) assay was used to evaluate the antioxidant activities of compounds **4c**, **4g**, **4n**, **5c**, **5d**, and **5i** using the colorimetric method. Trolox,[60] a water-soluble vitamin E analogue, was used as a standard, and the antioxidant activity was expressed as Trolox equivalent (TAC value = 1.00). As shown in Table 4,

Table 4. Total Antioxidant Capacity and Neurotoxicity for Promising Compounds

compd.	total antioxidant capacity (Trolox equivalent)[a]	SH-SY5Y cytotoxicity IC$_{50}$ (μM)
4c	0.80 ± 0.032	27.94 ± 1.24
4g	1.32 ± 0.051	85.97 ± 3.81
4n	0.66 ± 0.026	91.66 ± 4.06
5c	0.88 ± 0.034	36.28 ± 1.43
5d	1.10 ± 0.043	71.06 ± 2.8
5i	1.12 ± 0.044	17.22 ± 0.76

[a]The data are expressed as μmol of Trolox equivalent/μmol tested compound.

most compounds showed moderate to strong antioxidant activities, with TAC values ranging from 0.66 to 1.32. In particular, analogues **4g**, **5i**, and **5d** showed the most potent antioxidant activities with TAC values of 1.32, 1.12, and 1.10 Trolox equivalents, respectively.

2.2.7. In Vitro Neurotoxicity Assay. The cytotoxicity of the most potent and selective inhibitors **4c**, **4g**, **4n**, **5c**, **5d**, and **5i** was screened against human neuroblastoma SH-SY5Y cells (Table 4). The toxicity assay was investigated using the 3-(4,5-dimethylthiazole-2-yl)-2,5-diphenyltetrazolium bromide (MTT) assay.[61] Calculated IC$_{50}$ values of tacrine-chromeno-aryl sulfonate conjugates **4c**, **4g**, and **4n** were in the range from 27.94 to 91.66 μM, while tacrine-chromeno-acetophenone derivatives displayed IC$_{50}$ values from 17.22 to 71.06 μM. From these results, it was concluded that most of the promising compounds had a wide therapeutic safety range at their active concentration against their targets as represented in Tables 1−3.

2.2.8. In Vitro Hepatotoxicity Assay. As implied in the Introduction section, tacrine was the first FDA-approved anti-AD drug and it was stopped due to hepatotoxicity.[62] Thus, it is important to evaluate the hepatotoxicity of compounds **4c**, **4g**, **4n**, **5c**, **5d**, and **5i** using the HepG2 cell line *via* an MTT assay in comparison to tacrine and doxorubicin (as a reference

cytotoxic agent). All of the tested compounds demonstrated 100% cellular viability at their IC_{50} values. Chloroacetophenone derivatives **5c** and **5d** were enormously safe to liver cells when compared to other compounds with IC_{50} values of 188.20 and 154.10 μM, respectively. Moreover, the methoxysulfonate compound **4g** and the acetophenone compound **5i** also had high safety with IC_{50} values of 126.20 and 112.70 μM, respectively. Sulfonates **4c** and **4n** had wide safety on liver cells with IC_{50} values of 78.29 and 67.37 μM, respectively. The calculated IC_{50} values highlighted that chloroacetophenone derivatives had promising safety over sulfonate derivatives. The safety index ratio (SI) hepatotoxicity IC_{50}/AChE IC_{50} was calculated to be ranging from 125.26 to 611.51, which revealed that compounds **4c**, **4g**, **4n**, **5c**, **5d**, and **5i** had an accepted cytotoxicity at their therapeutic IC_{50} values (Table 5).

Table 5. *In Vitro* Hepatotoxicity and Safety Index Ratio of Promising Compounds[b]

compd. no.	HepG2 cytotoxicity $IC_{50} \pm SD$ (μM)	AChE inhibition $IC_{50} \pm SD$ (μM)	safety index ratio (SI)[a]
4c	78.29 ± 3.6	0.62 ± 0.03	125.26
4g	126.20 ± 5.3	0.30 ± 0.01	417.88
4n	67.37 ± 3.3	0.47 ± 0.02	141.53
5c	188.20 ± 6.9	0.44 ± 0.02	427.73
5d	154.10 ± 6.2	0.25 ± 0.01	611.51
5i	112.70 ± 5.1	0.56 ± 0.03	200.53
Tacrine	17.5 ± 1.1	0.19 ± 0.01	92.11
Doxorubicin	4.50 ± 0.2	ND	ND

[a]Safety index is the ratio of hepatotoxicity IC_{50} to AChE IC_{50}. [b]ND, not determined.

2.2.9. Metal Chelation Properties. In AD patients, changes in the dynamic balance of the metal ions in the brain are closely related to Aβ deposition and tau hyperphosphorylation, suggesting a crucial role of the metal ions in the pathogenesis of AD.[63,64] The ability of the tested compounds to chelate to metals might prevent neurodegeneration and oxidative stress, which were accompanied by β-deposition. The potential of the most active AChE inhibitors **4c**, **4g**, **4n**, **5c**, **5d**, and **5i** to chelate metals like Fe^{+2}, Cu^{+2}, and Zn^{+2} was explored using UV−vis spectroscopy, and the results are shown in Figure 4. In the absence of metal ions, compound **4c** gave absorbance at 225 nm, while upon the addition of $FeSO_4$, $CuSO_4$, and $ZnSO_4$, extraordinary hyperchromic shifts were obtained, which alludes to the formation of complexes with the corresponding metal ions. Compound **4g** displayed hyperchromic shifts at 243 nm when treated with $FeSO_4$ and $CuSO_4$ solutions, whereas it displayed a slight hypochromic shift with $ZnSO_4$ solution. A remarkable hyperchromic effect was shown in the spectrum of compound **4n** when mixed with $FeSO_4$, $CuSO_4$, and $ZnSO_4$ solutions. Compound **5c** exhibited a noteworthy hyperchromic effect with Fe^{+2} and Cu^{+2} and a slight hyperchromic effect with Zn^{+2}. In the metal-free condition, compound **5d** showed an absorbance peak at 229 nm, and a noticeable optical shift was detected after adding $FeSO_4$, which alludes to the formation of the **5d**−Fe(II) complex, while it exhibited a slight hyperchromic shift with $CuSO_4$ and $ZnSO_4$ solutions. Compound **5i** displayed a hyperchromic effect with $FeSO_4$ only without remarkable shifts with $CuSO_4$ and $ZnSO_4$. The changes in the absorbances suggest the formation of a compound−metal complex, and the chelating ability could be due to biometal complex formation through the coordinate bonds with the functional groups such as nitro, carbonyl, sulfonate, or amine.[65,66]

2.2.10. Blood−Brain Barrier (BBB) Prediction. The permeability of the blood−brain barrier (BBB) is an important measure for compounds that target CNS. A CBLigand-BBB prediction server was used to predict BBB permeability of the most active compounds from this point. This calculator combines two algorithms, AdaBoost and Support Vector
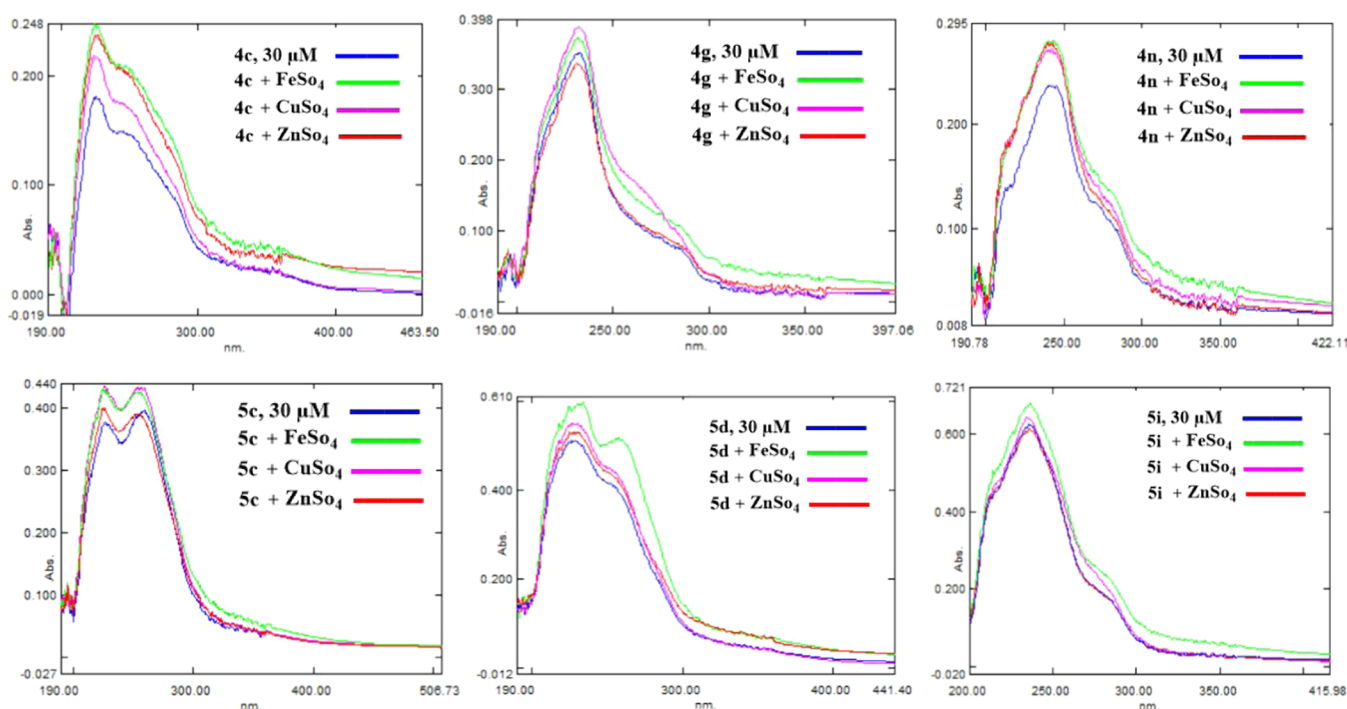
Figure 4. UV spectra of compounds **4c**, **4g**, **4n**, **5c**, **5d**, and **5i** (30 μM) in the presence of $CuSO_4$, $ZnSO_4$, and $FeSO_4$ (30 μM) in ethanol.
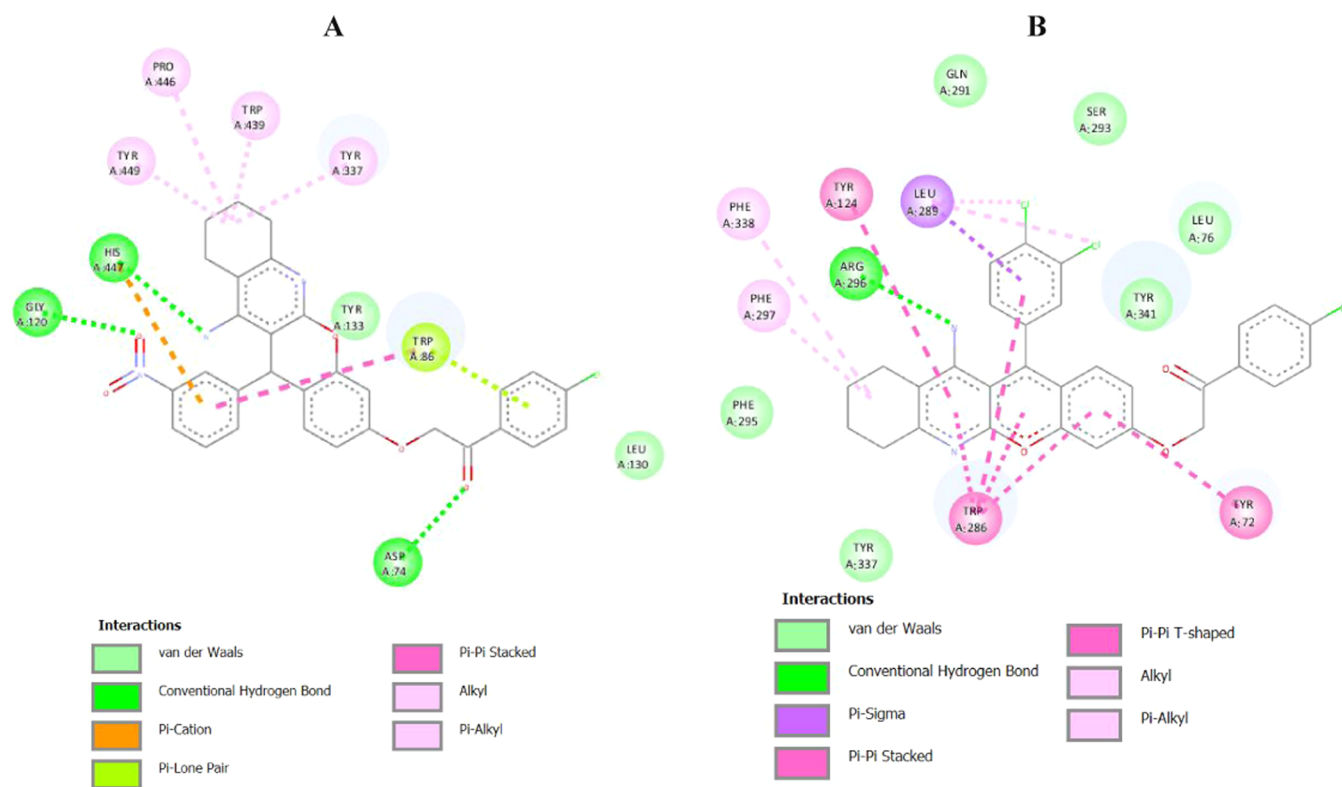
Figure 5. Two-dimensional (2D) representation of docking poses for the compounds **5c** (A) and **5d** (B) in the active site of AChE (PDB code: 4BDT).

Machine, with four different fingerprints to predict whether a compound will pass the BBB (+) or cannot (−).[67] From Table 1, all calculations for the synthesized compounds were found to be BBB (+), which is essential for exerting their biological activities in the brain.

2.3. Choice of Candidates. Based on the results of the previous biological evaluations, compounds **5c** and **5d** exhibited the most desirable multiple functions for Alzheimer's disease. They were forceful hAChE inhibitors with IC_{50} values of 0.44 and 0.25 μM, respectively. Furthermore, they considered potent BuChE inhibitors, particularly compound **5c**, which was 10-fold more active than rivastigmine (IC_{50} = 0.08 versus 0.81 μM). Moreover, they had the ability to bind PAS, influencing Aβ aggregation and decreasing Aβ-related neurodegeneration, especially compound **5d**, which was 8-fold more active than curcumin with 76% inhibition at 10 μM. Additionally, **5c** and **5d** showed balance and significant enzyme inhibition potential against BACE-1 at the submicromolar level with IC_{50} values of 0.38 and 0.44 μM, respectively. However, their inhibitory activities toward the MAO-B enzyme showed IC_{50} values of 5.15 and 2.42 μM, respectively. Also, both compounds exhibited good antioxidant activities and remarkable abilities to chelate metals like Fe^{+2}, Zn^{+2}, and Cu^{+2}, which may inhibit oxidative stress in the brains of AD patients. Besides, they were safe toward SH-SY5Y normal cells and the HepG2 cell line, along with their positive scoring of BBB permeability.

These properties highlighted that compounds **5c** and **5d** could serve as new multifunctional candidates for further development in the treatment of AD, so they were selected for *in silico* molecular modeling simulations including docking into hAChE, hBuChE, BACE-1, MAO-B, and Aβ_{1-42} to explain the biological experimental results.

3. DOCKING STUDIES

Molecular modeling of the selected compounds **5c** and **5d** was conducted to explore their binding modes and interactions with the constitutive amino acids in the active sites of AChE, BuChE, BACE-1, MAO-B, and Aβ_{1-42} and to determine the effects of their structural modification on their inhibitory action. Autodock software version 2012 was used for the docking[68,69] study, and Discovery Studio Visualizer 2021 was used for viewing and analyzing ligand interactions. The three-dimensional (3D) docking panels are represented in Tables S20−S24 (Supporting Information).

3.1. Docking into the Active Site of the hAChE Enzyme. Molecular modeling of the most active AChE inhibitors **5c** and **5d** into the binding pocket of hAChE cocrystallized with fasciculin 2 (FAS-2) and huprine W (PDB code: 4BDT) was performed. The active site of hAChE is composed of the catalytic triad (Ser203, Glu334, and His447) at the bottom of the gorge, while the anionic subsite is at Trp86, Tyr133, Tyr337, and Phe338. The acyl pocket is at Phe295 and Phe297, but the oxyanion hole is at Gly120, Gly121, and Ala204. In addition to this, the peripheral anionic site (PAS) of AChE lies at the entrance to the active site gorge. It is composed of five residues Tyr72, Trp286, Asp74, Tyr124, and Tyr341.[70] Amino acids Tyr72 and Trp286 are of particular interest as they are believed to play a major role in Aβ plaque formation, which is a key step in the development of AD.[71]

As shown in Figure 5, the docking result of compound **5c** (binding energy = −10.14 kcal/mol) showed three conventional hydrogen bonds: between the catalytic amino acid His447 and the free amine moiety, the carbonyl group and Asp74 in the peripheral anionic site, and oxygen of the nitro moiety and Gly120 in the oxyanion hole. The phenyl moiety
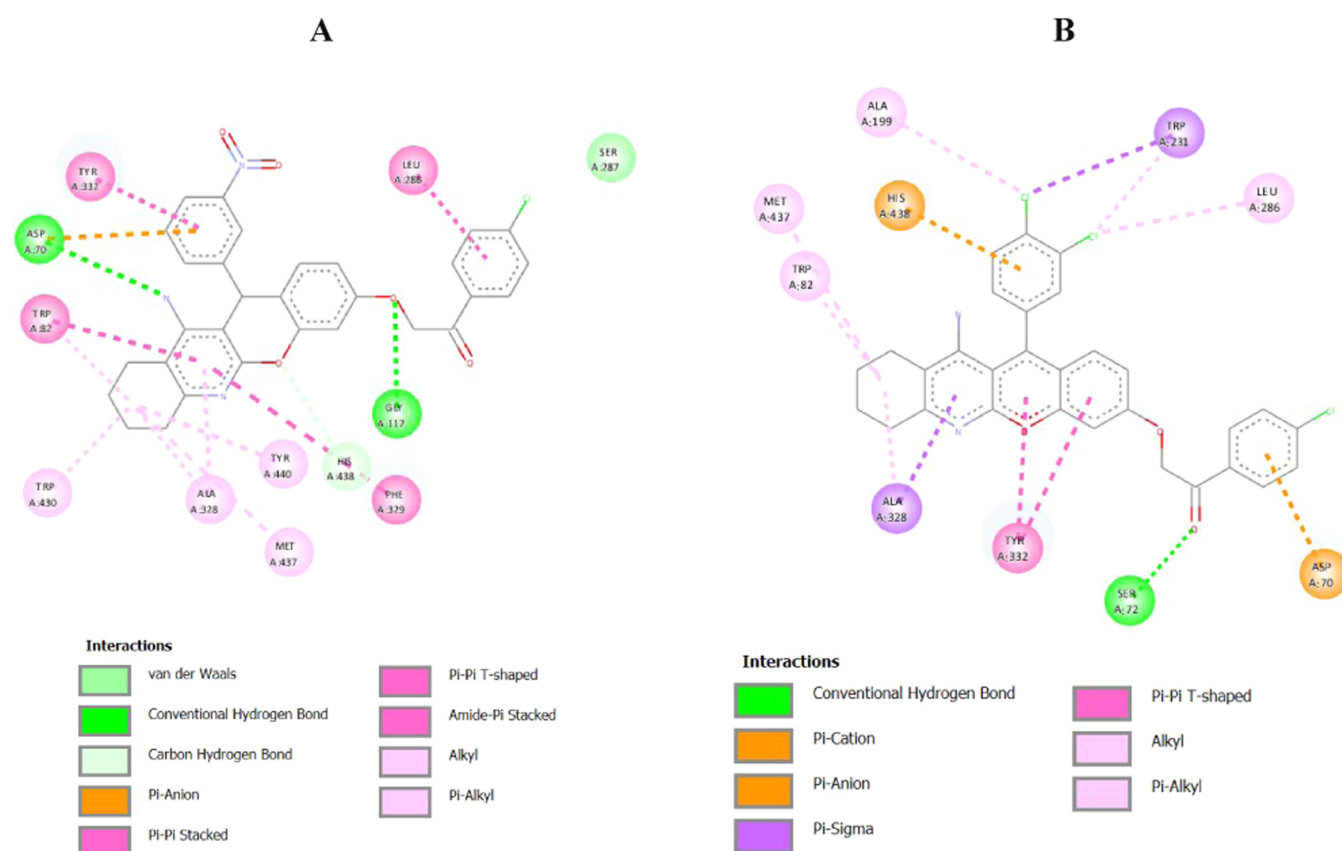
Figure 6. 2D representation of docking poses for the compounds **5c** (A) and **5d** (B) in the active site of BuChE (PDB code: 4BDs).

adopted an appropriate orientation to bind to the catalytic Trp86 and His447, establishing pi−pi stacking, pi−lone pair, and pi−cation interactions, respectively. The cyclohexyl ring of the planner tetrahydroquinoline (THQ) formed a hydrophobic alkyl and π−alkyl interaction with Tyr449, Pro446, Trp439, and the catalytic amino acid Tyr337. Besides, it displayed van der Waals interactions with leu130 and Tyr133 (PAS residue).

The most active compound **5d** (binding energy = −10.69 kcal/mol) showed an attractive force with the binding pocket of the *h*AChE enzyme by binding to the CAS site through hydrophobic pi−alkyl interactions between the cyclohexyl of THQ and Phe338 in the catalytic active site and Phe297 in the acyl pocket. The indole ring of Trp286 in PAS stacked against the planner pyridine ring of THQ, chromene, and the peripheral phenyl group by strong arene−arene interactions. The benzene ring of the chromene moiety formed pi−pi T-shaped interactions with the Tyr72 PAS residue, while the pyridine group interacted with the Tyr123 residue. The Cl substituent on the benzene ring of **5d** formed alkyl and halogen (chlorine) interactions with the Leu289 residue. Finally, it formed van der Waals interactions with Gln291, Ser293, Leu76, Tyr337 (CAS), phe295 (acyl pocket), and Tyr341 (PAS) residues.

Taken together, all of these results indicated that compounds **5c** and **5d** could bind simultaneously to both the PAS and the CAS sites. Given the ability to inhibit both CAS and PAS, it may be understandable why they showed the most potent activity in the enzyme assay.

3.2. Docking into the Active Site of the *h*BuChE Enzyme. The catalytic triad of the active site of BuChE is composed of Ser198, His438, and Glu325 in the esteratic site of the active center, while at the bottom of the gorge, it is the anionic subsite at Trp82. Leu286, Val288, and Trp231 are found in the acyl-binding pocket of BuChE, where the oxyanion hole found near the choline-binding site includes Gly116, Gly117, and Ala199. The peripheral anionic site (PAS) is located at the mouth of the gorge with Asp70 and Tyr332 residues.[72,73] Molecular modeling of the most active BuChE inhibitors and also the selected compounds **5c** and **5d** was performed. The crystal complex of BuChE with tacrine (PDB code: 4BDs) was selected for the docking research.

As displayed in Figure 6, the obtained docking results of compound **5c** (binding energy = −12.17 kcal/mol) showed that it bound to the anionic substrate binding site residue Trp82 by the THQ moiety *via* pi−pi stacking and pi−alkyl hydrophobic interactions. His438 in CAS was attached to the oxygen of chromene by a carbon−hydrogen interaction. **5c** formed two conventional hydrogen bonds with the PAS residue Asp70 *via* the free amino group and the oxyanion hole residue Gly117 *via* the oxygen of the acetophenone moiety. Leu286 in the acyl-binding pocket interacted with the terminal benzene by amide−pi stacking. The peripheral benzene moiety reacted by pi−pi and pi−anion interactions with the PAS residues Tyr332 and Asp70, respectively. Finally, the cyclohexyl of the THQ moiety formed several lipophilic interactions with Met437, Tyr440, Trp430, and Ala328, while the pyridine ring attached to Phe329 by a pi−pi T-shaped stacking. Briefly, it is noteworthy to say that compound **5c** interacted with important amino acid residues in the PAS, oxyanion hole, esteratic site, and anionic substrate active sites of BuChE,
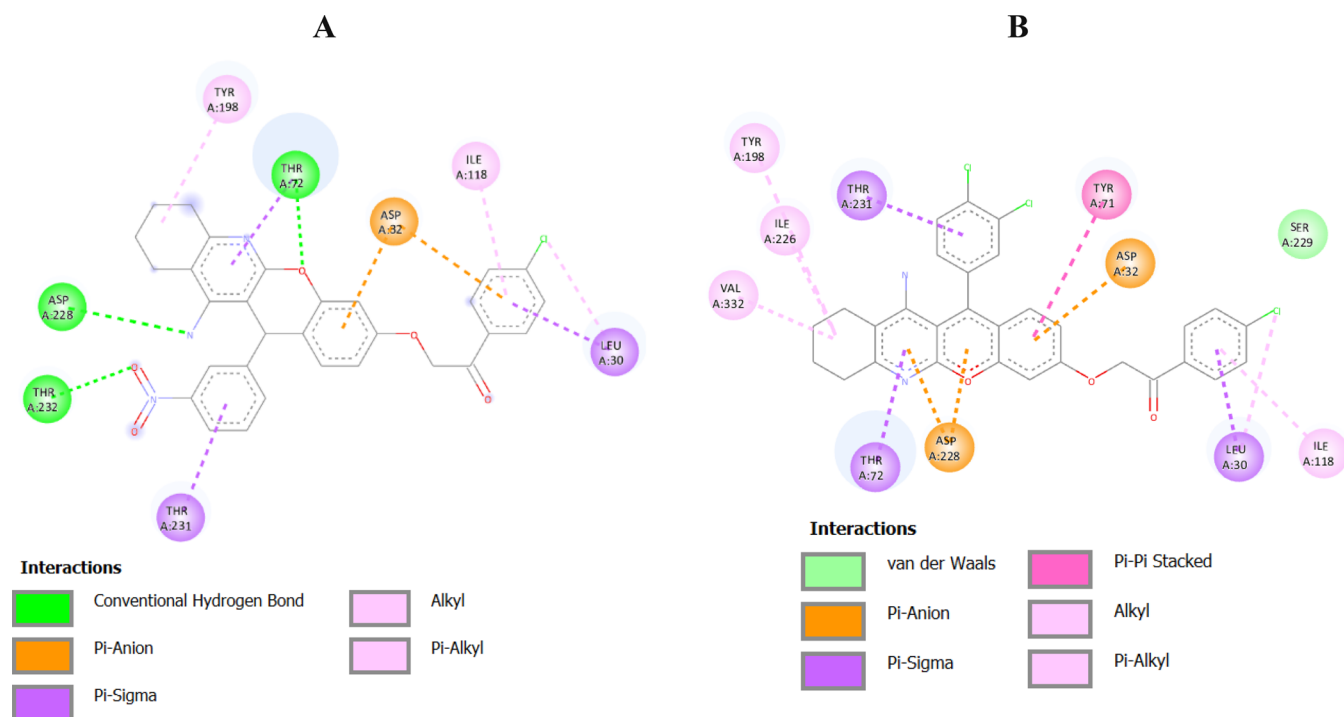
Figure 7. 2D representation of docking poses for compounds **5c** (A) and **5d** (B) in the active site of BACE-1 (PDB code: 2ZJM).
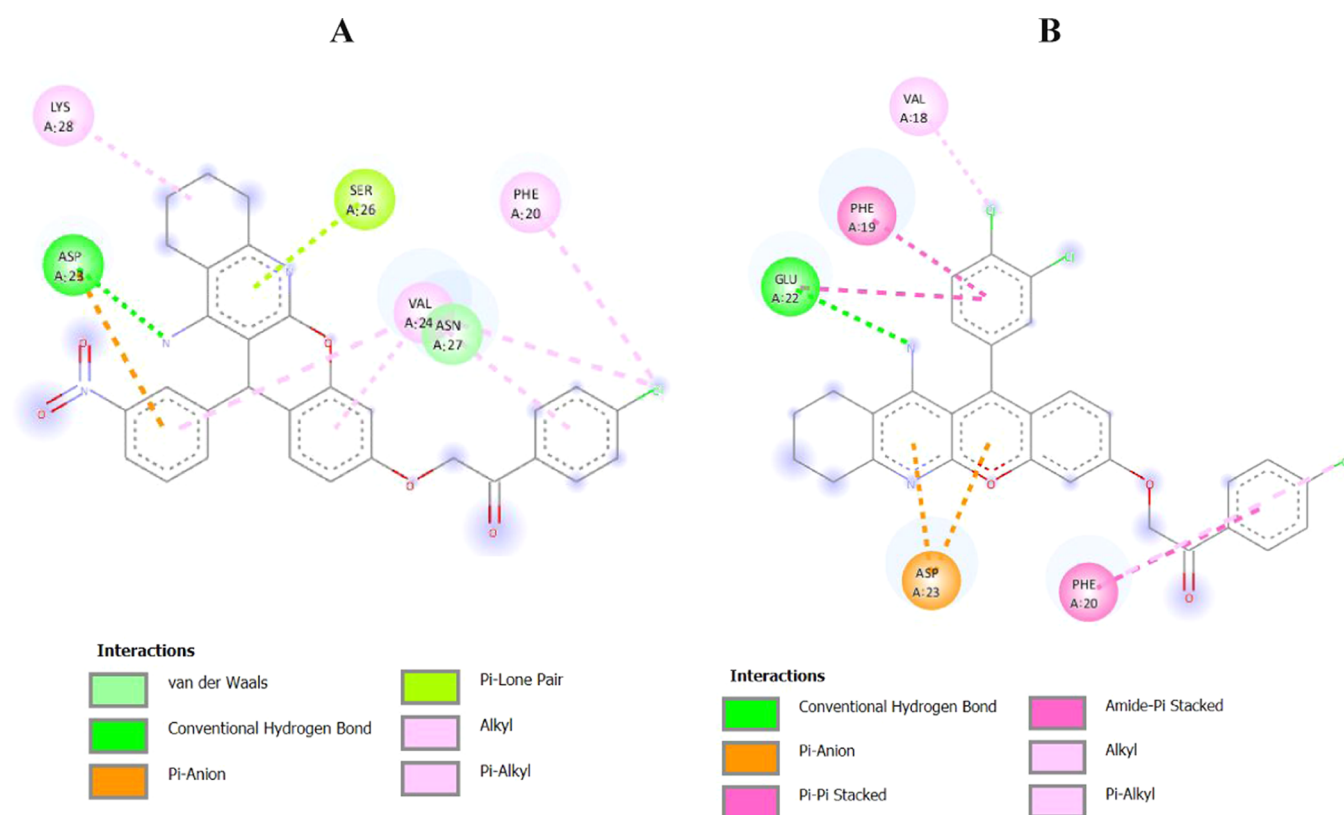
Figure 8. 2D representation of docking poses for the compounds **5c** (A) and **5d** (B) in the active site of the β amyloid (PDB code: 6SZF).

which explains its noteworthy BuChE inhibitory activity (IC$_{50}$ = 0.082 μM).

Considering compound **5d** (binding energy = −11.71 kcal/mol), the catalytic Trp82 was bound to cyclohexyl by a pi−alkyl hydrophobic interaction, while Met437 and Ala328 were stacked by alkyl hydrophobic interactions. Pi−sigma stacking of the pyridine of THQ with Ala328 was noted. The peripheral benzene ring was attached to the key amino acid His438 in the CAS by a pi−cation bond. Cl atoms participated with hydrophobic alky and pi−alkyl interactions with Ala199 in the oxyanion hole and Trp231 and Leu286 in the acyl pocket. Trp231 was also bound by a pi−sigma interaction. **5d** bound
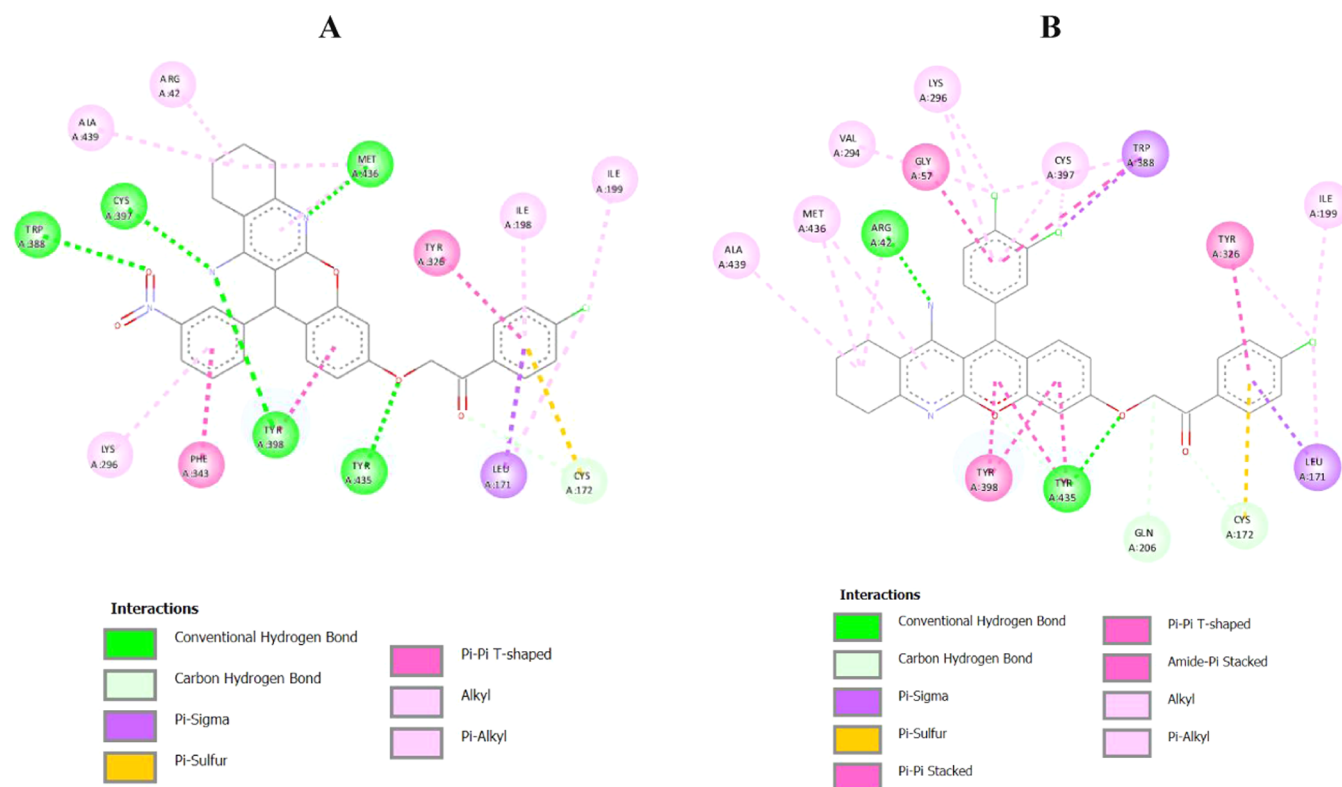
Figure 9. 2D representation of docking poses for the compounds (pink color) **5c** (A) and **5d** (B) in the active site of MAO-B (PDB code: 2V5Z) with the FAD cofactor.

to the PAS residue Tyr332 by an arene−arene T-shaped stacking with the chromene moiety. A conventional hydrogen bond between carbonyl and the Ser72 residue was observed. The PAS residue Asp70 was bound to the terminal benzene ring in terms of a pi−anion interaction. These results explained that **5d** effectively occupied the active site, PAS, and extended to bind with the CAS.

3.3. Docking into the Active Site of the BACE-1 Enzyme. The lead compounds **5c** and **5d** were observed against BACE-1, and the results are shown in Figure 7. PDB ID: 2ZJM was applied to establish the starting docking model of BACE-1 with F1M. The catalytic dyad of BACE-1 consisted of two aspartic acid residues: Asp32 and Asp228.[74]

Compound **5c** (binding energy = −10.17 kcal/mol) stabilized by three conventional hydrogen bonds, with the key amino acid Asp228 to the free amino moiety, Thr72 to the oxygen of the chromene group, and Thr232 to the oxygen of the nitro moiety. π−anion interactions with the catalytic Asp32 to the phenyl ring of chromene and the terminal benzene ring were characteristics of **5c**. It formed two pi−sigma interactions with Thr231 and Leu30 and three hydrophobic alkyl and pi−alkyl interactions with Leu30, Tyr198, and Ile118.

Compound **5d** (binding energy = −11.75 kcal/mol) showed several pi−anion interactions with prominent amino acid residues Asp32 and Asp228 to the chromene moiety and pyridine of the THQ ring. Several pi−sigma interactions were established to Thr231, Thr72, and Leu30. Notably, a π−π stacking was revealed between the benzene ring of chromene and the Tyr71 residue. Hydrophobic interactions (alkyl and pi−alkyl) to Ile118, Ile226, Tyr226, and Val332 were observed; in addition, the Cl substituent on the terminal benzene ring formed an alkyl hydrophobic interaction with Leu30.

3.4. Docking into the Aβ$_{1−42}$ Binding Pocket. Blocking of or interfering with the aggregation of Aβ and β-sheet construction using small organic molecules that selectively bind or inhibit Aβ aggregates is a promising strategy for treatment of AD.[75] Asp23, Glu22, and Lys28 salt bridge formation and hydrophobic interactions with Phe20, Glu22, Asp23, Gly29, and Ala30 residues are crucial for stabilization of β-sheet construction.[76] Lead compounds **5c** and **5d** were selected for molecular modeling research in the Aβ$_{1−42}$ binding pocket using the PDB code: 6SZF [76] (Figure 8).

Compound **5c** (binding energy = −10.02 kcal/mol) exhibited intermolecular hydrogen bonding between the catalytic amino acid Asp23 and H of the free amino group. Additionally, Asp23 formed a pi−anion interaction with the phenyl ring. The pi−lone pair interaction appeared between Ser26 and the pyridine ring. **5c** bound to Phe20, Lys28, and Val24 by hydrophobic interactions.

The most active compound **5d** (IC$_{50}$ = 0.77 μM) (binding energy = −10.76 kcal/mol) showed strong interaction in the active site of Aβ$_{1−42}$. The catalytic amino acid Glu22 showed a conventional hydrogen bond with the amino moiety and the amide−pi interaction with the peripheral phenyl ring. Furthermore, the catalytic amino acid Asp23 formed two arrays of pi−anion interactions with the pyridine and chromene rings. Strong arene−arene interactions were observed between the amino acids phe19 and Phe20 and the benzene rings. Ala18 established an alkyl hydrophobic bond with the chlorine atom.

Briefly, it was noteworthy to say that compounds **5c** and **5d** interacted with an array of important amino acid residues that participated in stabilizing the α-helical content and blocking the β-sheet construction. This clarifies the effectiveness of compounds **5c** and **5d** in inhibiting Aβ aggregation.

3.5. Docking into the Active Site of the MAO-B Enzyme. The *h*MAO-B enzyme has two cavities connected by the Ile-199 amino acid, which acts as a "gate". The entrance cavity is highly hydrophobic and the second contains the substrate binding pocket. At the end of this cavity is the FAD coenzyme. Based on the polyamine oxidase three-dimensional crystal structure, four key amino acids, Lys296, Trp388, Tyr398, and Tyr435, play important roles in the MAO catalytic activity. Lys296, Trp388, and Tyr398 in MAO-B are involved in the noncovalent binding to FAD.[77] The FAD as well as the two parallel tyrosyl key amino acids (398 and 435) establish an aromatic cage in the binding site.[78−80] Docking study of the lead compounds **5c** and **5d** was performed using a crystal (PDB ID: 2V5Z) (in complex with safinamide). Various reported studies indicated that binding with Tyr326, Ile-199, Tyr398, Lys296, Trp388, and Tyr435 residues is mainly noticed in most of the *h*MAO-B ligands; thus, it could be realized that they are crucial for the interaction with the enzyme.[77,81−83]

It can be seen from Figure 9 that ligand **5c** (binding energy = −12.96 kcal/mol) interacted by lipophilic interactions with Ile198, Ala439, Arg42, and the catalytic Lys296. Also, the gate amino acid Ile-199 bound with the chloro substituent on the terminal benzene ring by a pi−alkyl interaction, meaning it could block the entrance cavity and obstruct the entrance of any substrate to the cavity. Pi−Pi T-shaped interactions were observed between the terminal benzene ring and the key amino acid Tyr326 as well as between the peripheral phenyl ring with Phe343. Moreover, the chromene moiety interacted by a pi−pi-stacking interaction with the phenyl ring of Tyr398 in the aromatic cage of the pocket. Meanwhile, the NH_2 group displayed hydrogen-bond interactions with Cys397 and with the key residue Tyr398, while the N atom of THQ stacked with Met436. The oxygen of the nitro group exhibited hydrogen bonding with the catalytic residue Trp388. The $COCH_2O$ moiety interacted *via* a hydrogen bond with Tyr435 through the oxygen atom in the aromatic cage and *via* a carbon−hydrogen bond to Cys172 through the carbonyl moiety. The terminal benzene ring attached to Cys172 and Leu171 by means of pi−sulfur and pi−sigma interactions, respectively.

Regarding compound **5d** (binding energy = −13.66 kcal/mol), it bound with the gate residue *via* a hydrophobic alkyl interaction through a chlorine halogen atom in the terminal benzene ring. The chlorine atom also interacted with Tyr326 *via* a pi−alkyl interaction, while the benzene ring stacked to Tyr326 by a pi−pi T-shaped stacking. The key amino acid Tyr435 formed two arrays, pi−pi T-shaped interactions with the chromene moiety and a hydrogen-bond interaction with the oxygen group of the acetophenone moiety. However, the catalytic residue Tyr398 stacked to the chromene group *via* two arrays of arene−arene interactions. Interaction with Trp388 is very crucial in terms of catalytic activity; **5d** bound to typ388 by pi−pi T-shaped and pi−sigma interactions. Besides, the phenyl moiety also established alkyl and pi−alkyl interactions with the Lys296 catalytic residue. The free amino moiety established a hydrogen bond with Arg42. The $COCH_2O$ moiety was stabilized by two carbon−hydrogen bonds with Gln206 and Cys172. Hydrophobic interactions with Leu171, Cys172, Cys397, Val294, Met436, and Ala436 were detected.

From the 3D view of interactions of compounds **5c** and **5d** (Table S24, Supporting Information), it turned out that the compounds tightly interacted with the crucial amino acid residues covering the cavity and were positioned remarkably close to the FAD cofactor.

4. CONCLUSIONS

Given the complex pathogenesis of Alzheimer's disease (AD), the development of multitarget-directed ligands (MTDLs) has been used to address multiple factors involved in the progression of Alzheimer's disease. A novel series of tacrine-chromene derivatives were designed by the MTDL strategy; the derivatives were synthesized and evaluated to treat AD. Compounds **4c**, **4g**, **4n**, **5c**, **5d**, and **5i** exhibited the highest AChE inhibition potency and showed balanced and potent inhibition against BuChE, BACE-1, MAO-B, and β amyloid aggregation, in addition to antioxidant activity and optimum metal-chelating capability. The lead compounds **5c** and **5d** proved to be multifunctional agents for AD as they showed potent and selective inhibition AChE IC_{50} = 0.44 and 0.25 μM. Compound **5c** (BuChE IC_{50} = 0.08) was 10-fold more active than rivastigmine. Moreover, they had the ability to bind to PAS, influencing Aβ aggregation and decreasing Aβ-associated neurotoxicity, especially compound **5d**, which was 8 times more active than curcumin with IC_{50} = 0.74 μM and 76% inhibition at 10 μM. Compounds **5c** and **5d** showed strong BACE-1 inhibition at the submicromolar level with IC_{50} = 0.38 and 0.44 μM, which were double the activity of curcumin. They also had single-digit micromolar inhibitory activity against MAO-B with IC_{50} = 2.4 and 5.5 μM. Furthermore, they exhibited acceptable relative safety on the normal cell SH-SY5Y and HepG2 cell lines and showed satisfactory metal-chelating properties toward Fe^{+2}, Zn^{+2}, and Cu^{+2}, inhibiting oxidative stress in AD brains. Therefore, these results implied that compounds **5c** and **5d** were advanced multifunction agents and deserved further preclinical study against mild-to-severe Alzheimer's disease.

Molecular modeling simulations interpreted the biological results and shed light on the significance of the chromene moiety in designing AD targets due to their enormous binding to the active site of the target enzymes (ChE_S, BACE-1, and MOE-B) and A$\beta_{1−42}$.

5. EXPERIMENTAL SECTION

5.1. Chemistry. Melting points were recorded using the Stuart apparatus and were uncorrected. IR spectra were recorded on a Nicolet iS10 FT-IR spectrometer (v in cm^{-1}) using KBr discs. ^1H NMR and ^{13}C NMR spectra were recorded on a Bruker Avance III 400 spectrometer at the NMR Unit, Faculty of Pharmacy, Mansoura University, Egypt. Tetramethylsilane (TMS) was used as the internal standard, and all chemical shifts are expressed in ppm. Electron ionization mass spectrometry (EI MS) was performed on a Hewlett Packard 5988 spectrometer at Al-Azhar University, Cairo, Egypt. Microanalyses (C, H, N) were conducted at the Microanalytical Unit, Cairo University, and the results were within ±0.4% of the theoretical values. The metal chelation assay was achieved using a UV−visible Shimadzu spectrophotometer at the Faculty of Pharmacy, Mansoura University, Egypt. The HRMS analysis was recorded on LC/Q-TOF, 6530 (Agilent Technologies, Santa Clara, CA) equipped with an autosampler (G7129A), a quat. pump (G7104C), and a column comp (G7116A) at the Faculty of Pharmacy, Fayoum University, Egypt. *h*AChE, *h*BuChE, BACE-1, MAO-B, A$\beta_{1−42}$

self-aggregation inhibition assay, MTT cytotoxicity assay, and total antioxidant capacity (TAC) assay were conducted at the Holding Company for Biological Products and Vaccines (VACSERA), Cairo, Egypt. Compounds **1a−e** were previously reported.[47]

5.1.1. General Procedure for the Preparation of 2-Amino-4-(substituted)-7-hydroxy-4H-chromene-3-carbonitrile (2a−e).[48] In a 50 mL round-bottom flask, a mixture of arylidene malononitriles **1a−e** (1 mmol) and resorcinol (1 mmol) was refluxed in ethanol (15 mL) in the presence of a few drops of piperidine for 24 h. After the reaction was completed as judged by TLC, the reaction mixture was allowed to cool and then poured into crushed ice. The formed solid was filtered off, dried, and recrystallized from ethanol.

5.1.2. General Procedure for the Preparation of 11-Amino-12-substituated-7,9,10,12-tetrahydro-8H-chromeno-[2, 3-b]quinolin-3-ol (3a−e). In a 50 mL round-bottom flask, aluminum chloride (1.5 mmol, 0.2 g) was added into dry 1,2-dichloroethane (DCE) (10 mL) and heated at reflux for a few minutes. Then, a mixture of **2a−e** (1 mmol) and cyclohexanone (1.5 mmol, 0.147 g, 0.155 mL) was added into the reaction. The mixture was continuously refluxed for 3−5 h. After reaction completion as judged by TLC, the solvent was evaporated, water was added, and the mixture was adjusted to pH = 8−9 with 10% sodium hydroxide solution. After stirring for 30 min, the formed precipitate was filtered and washed with water. Purification by column chromatography on silica gel (petroleum ether/ethyl acetate = 3:1 then 1:1, v/v) afforded the title compounds **3a−e**.

5.1.2.1. Characterization of 11-Amino-12-(3-bromophenyl)-7,9,10,12-tetrahydro-8H-chromeno[2,3-b]quinolin-3-ol (3a). Yield = 86%, mp = 96−101 °C, yellow solid, IR (KBr, v, cm^{-1}): 3093 (OH), 3403 and 3490 (NH$_2$); ^{1}H NMR (400 MHz, DMSO-d_6): δ = 1.72 (s, 4H, 2CH$_2$), 2.29 (m, 2H, CH$_2$), 2.59 (s, 2H, CH$_2$), 5.27 (s, 1H, CH of pyran), 5.64 (s, 2H, NH$_2$; D$_2$O exchangeable), 6.47 (d, J = 2.36 Hz, 1H, ArH), 6.50 (m, 1H, ArH), 6.98 (d, J = 8.2 Hz, 1H, ArH), 7.19 (d, J = 5.0 Hz, 2H, ArH), 7.33 (m, 1H, ArH), 7.51 (s, 1H, ArH), 9.59 (s, 1H, OH; D$_2$O exchangeable); ^{13}C NMR (100 MHz, DMSO-d_6): δ = 22.59, 22.81, 23.45, 32.52, 38.49, 98.57, 103.24, 111.80, 112.55, 115.76, 122.10, 126.70, 129.63, 129.91, 130.17, 131.29, 149.28, 151.76, 151.82, 152.99, 155.77, 157.63; MS (EI) m/z (C$_{22}$H$_{19}$N$_2$O$_2$Br): 425.26 (M$^+$ + 2, 2.38%), 424.30 (M$^+$ + 1, 2.06%), 423.31 (M$^+$, 3.78%), 89.08 (100%); elemental analysis for C$_{22}$H$_{19}$N$_2$O$_2$Br, calcd: C, 62.42; H, 4.52; N, 6.62; found: C, 62.00; H, 4.49; N, 6.61.

5.1.2.2. Characterization of 11-Amino-12-(3-methoxyphenyl)-7,9,10,12-tetrahydro-8H-chromeno[2, 3-b]quinolin-3-ol (3b). Yield = 91%, mp = 106−111 °C, yellow solid, IR (KBr, v, cm^{-1}): 3450 (OH), 3405 and 3493 (NH$_2$); ^{1}H NMR (400 MHz, DMSO-d_6): δ = 1.72 (s, 4H, 2CH$_2$), 2.29 (m, 2H, CH$_2$), 2.59 (s, 2H, CH$_2$), 3.69 (s, 3H, OCH$_3$), 5.19 (s, 1H, CH of pyran), 5.52 (s, 2H, NH$_2$; D$_2$O exchangeable), 6.45 (d, J = 2.1 Hz, 1H, ArH), 6.48 (d, J = 2.8 Hz, 1H, ArH), 6.70 (dd, J = 1.8, 8.1 Hz, 1H, ArH), 6.75 (d, J = 7.8 Hz, 1H, ArH), 6.92 (s, 1H, ArH), 6.99 (d, J = 8.2 Hz, 1H, ArH), 7.13 (t, J = 7.9 Hz, 1H, ArH), 9.53 (s, 1H, OH; D$_2$O exchangeable); ^{13}C NMR (100 MHz, DMSO-d_6): δ = 22.63, 22.87, 23.44, 32.53, 38.89, 55.17, 98.45, 103.11, 111.27, 111.43, 112.41, 114.11, 119.85, 116.25, 129.90, 130.01, 136.05, 147.81, 148.12, 151.83, 152.71, 157.42, 159.66; MS (EI) m/z (C$_{23}$H$_{22}$N$_2$O$_3$): 305.8 (M$^+$ + 1, 3.14%), 304.97 (M$^+$, 1.83%), 114.01 (100%);

elemental analysis for C$_{23}$H$_{22}$N$_2$O$_3$, calcd: C, 73.78; H, 5.92; N, 7.48; found: C, 73.72; H, 5.95; N, 7.40.

5.1.2.3. Characterization of 11-Amino-12-(3-nitrophenyl)-7,9,10,12-tetrahydro-8H-chromeno[2, 3-b]quinolin-3-ol (3c). Yield = 86%, mp = 91−96 °C, yellow solid, ^{1}H NMR (400 MHz, DMSO-d_6): δ = 1.71 (s, 4H, 2CH$_2$), 2.28 (m, 2H, CH$_2$), 2.58 (s, 2H, CH$_2$), 5.49 (s, 1H, CH of pyran), 5.76 (s, 2H, NH$_2$; D$_2$O exchangeable), 6.48 (dd, J = 2.3, 8.3 Hz, 1H, ArH), 6.53 (d, J = 2.3 Hz, 1H, ArH), 7.00 (d, J = 8.3 Hz, 1H, ArH), 7.54 (t, J = 7.9 Hz, 1H, ArH), 7.62 (d, J = 7.8 Hz, 1H, ArH), 8.01 (d, J = 7.9 Hz, 1H, ArH), 8.26 (s, 1H, ArH), 9.66 (s, 1H, OH; D$_2$O exchangeable); ^{13}C NMR (100 MHz, DMSO-d_6): δ = 22.57, 22.80, 23.45, 32.54, 38.39, 98.38, 103.36, 111.96, 112.64, 115.35, 121.93, 122.00, 129.96, 130.65, 134.38, 148.13, 148.70, 151.87, 151.91, 153.21, 155.76, 157.81; elemental analysis for C$_{22}$H$_{19}$N$_3$O$_4$, calcd: C, 67.86; H, 4.92; N, 10.79; found: C, 67.80; H, 4.88; N, 10.71.

5.1.2.4. Characterization of 11-Amino-12-(3,4-dichlorophenyl)-7,9,10,12-tetrahydro-8H-chromeno[2, 3-b]quinolin-3-ol (3d). Yield = 86%, mp = 95−100 °C, yellow solid, IR (KBr, v, cm^{-1}): 3123 (OH), 3399 and 3491 (NH$_2$); ^{1}H NMR (400 MHz, DMSO-d_6): δ = 1.72 (s, 4H, 2CH$_2$), 2.30 (m, 2H, CH$_2$), 2.59 (s, 2H, CH$_2$), 5.31 (s, 1H, CH of pyran), 5.68 (s, 2H, NH$_2$; D$_2$O exchangeable), 6.48 (d, J = 8.2 Hz, 1H, ArH), 6.51 (d, J = 2.1 Hz, 1H, ArH), 7.00 (d, J = 8.2 Hz, 1H, ArH), 7.12 (dd, J = 1.9, 8.4 Hz, 1H, ArH), 7.49 (d, J = 8.4 Hz, 1H, ArH), 7.62 (d, J = 1.9 Hz, 1H, ArH), 9.62 (s, 1H, OH; D$_2$O exchangeable); ^{13}C NMR (100 MHz, DMSO-d_6): δ = 22.58, 22.80, 23.45, 32.53, 38.00, 98.20, 103.28, 111.89, 112.60, 115.26, 127.94, 129.34, 129.41, 129.94, 131.18, 131.37, 147.54, 151.74, 151.86, 153.15, 155.68, 157.75; MS (EI) m/z (C$_{22}$H$_{18}$N$_2$O$_2$Cl$_2$): 415.40 (M$^+$ + 2, 23.36%), 413.67 (M$^+$, 31.48%), 163.28 (100%); HRMS (m/z): [M + H]$^+$ calcd for C$_{22}$H$_{18}$N$_2$O$_2$Cl$_2$: 413.0818; found: 413.0809; elemental analysis for C$_{22}$H$_{18}$N$_2$O$_2$Cl$_2$, calcd: C, 63.93; H, 4.39; N, 6.78; found: C, 63.95; H, 4.45; N, 6.69.

5.1.2.5. Characterization of 11-Amino-12-(2-methoxyphenyl)-7, 9, 10, 12-tetrahydro-8H-chromeno[2, 3-b]-quinolin-3-ol (3e). Yield = 86%, mp = 103−108 °C, yellow solid, IR (KBr, v, cm^{-1}): 3250 (OH), 3382 and 3486 (NH$_2$); ^{1}H NMR (400 MHz, DMSO-d_6): δ = 1.71 (s, 4H, 2CH$_2$), 2.26 (m, 2H, CH$_2$), 2.57 (s, 2H, CH$_2$), 3.92 (s, 3H, OCH$_3$), 5.26 (s, 2H, NH$_2$; D$_2$O exchangeable), 5.42 (s, 1H, CH of pyran), 6.41 (dd, J = 2.4, 8.3 Hz, 1H, ArH), 6.48 (d, J = 2.3 Hz, 1H, ArH), 6.81 (t, J = 7.2 Hz, 1H, ArH), 6.88 (t, J = 1.4 Hz, 1H, ArH), (s, 1H, ArH), 7.04 (d, J = 7.9 Hz, 1H, ArH), 7.14 (m, 1H, ArH), 9.52 (s, 1H, OH; D$_2$O exchangeable); ^{13}C NMR (100 MHz, DMSO-d_6): δ = 22.58, 22.84, 23.34, 31.98, 32.46, 56.46, 98.98, 102.86, 111.61, 111.93, 112.25, 115.81, 121.89, 127.99, 129.89, 130.00, 134.32, 151.57, 151.90, 152.56, 155.42, 155.89, 157.33; elemental analysis for C$_{23}$H$_{22}$N$_2$O$_3$, calcd: C, 73.87; H, 5.92; N, 7.48; found: C, 73.80; H, 5.88; N, 7.39.

5.1.3. General Procedure for the Preparation of 11-Amino-12-(substituted)-7,9,10,12-tetrahydro-8H-chromeno-[2, 3-b]quinolin-3-yl-4-substituated-benzenesulfonate (4a−t). In a 50 mL round-bottom flask, a mixture of compounds **3a−e** (1 mmol), aryl sulfonyl chlorides (1 mmol), and K$_2$CO$_3$ (2 mmol, 0.27 g) was heated in acetone (10 mL) under reflux for 3−5 h and the reaction was monitored by TLC at a constant temperature. After completion of the reaction, the mixture was filtrated, and the solvent was evaporated under vacuum. The formed precipitate was purified by column

chromatography on silica gel (petroleum ether/ethyl acetate = 3:1 then 1:1, v/v) to afford the title compounds **4a−t**.

5.1.3.1. Characterization of 11-Amino-12-(3-bromophenyl)-7,9,10,12-tetrahydro-8H-chromeno[2, 3-b]quinolin-3-yl-4-fluorobenzenesulfonate (4a). Yield = 85%, mp = 210−215 °C, yellow solid, IR (KBr, v, cm^{-1}): 1379 (S=O), 3402 and 3502 (NH$_2$); ^{1}H NMR (400 MHz, DMSO-d_6): δ = 1.72 (s, 4H, 2CH$_2$), 2.29 (m, 2H, CH$_2$), 2.59 (s, 2H, CH$_2$), 5.42 (s, 1H, CH of pyran), 5.75 (s, 2H, NH$_2$; D$_2$O exchangeable), 6.77 (dd, J = 2.2, 8.4 Hz, 1H, ArH), 6.86 (d, J = 2.2 Hz, 1H, ArH), 7.16 (d, J = 7.8 Hz, 1H, ArH), 7.20 (d, J = 7.8 Hz, 1H, ArH), 7.25 (t, J = 8.5 Hz, 1H, ArH), 7.36 (d, J = 7.7 Hz, 1H, ArH), 7.51 (d, J = 8.7 Hz, 1H, ArH), 7.54 (d, J = 4.1 Hz, 2H, ArH), 7.97 (dd, J = 5.0, 8.7 Hz, 2H, ArH); ^{13}C NMR (100 MHz, DMSO-d_6): δ = 22.51, 22.74, 23.46, 32.51, 38.57, 97.61, 110.95, 113.13, 117.59, 117.82, 122.26, 124.73, 126.69, 130.11, 130.26, 130.72, 130.86, 131.52, 132.10, 132.20, 147.96, 148.49, 151.62, 151.98, 153.37, 155.24, 164.82, 167.35; MS (EI) m/z (C$_{28}$H$_{22}$N$_2$O$_4$BrSF): 582.86 (M$^+$ + 2, 25.57%), 582.06 (M$^+$ + 1, 42.63%), 581.05 (M$^+$, 33.65%), 173.65 (100%); elemental analysis for C$_{28}$H$_{22}$N$_2$O$_4$BrFS, calcd: C, 57.84; H, 3.81; N, 4.82; found: C, 57.82; H, 3.78; N, 4.79.

5.1.3.2. Characterization of 11-Amino-12-(3-methoxyphenyl)-7,9,10,12-tetrahydro-8H-chromeno[2, 3-b]quinolin-3-yl-4-fluorobenzenesulfonate (4b). Yield = 87%, mp = 125−130 °C, yellow solid, IR (KBr, v, cm^{-1}): 1380 (S=O), 3414 and 3502 (NH$_2$); ^{1}H NMR (400 MHz, DMSO-d_6): δ = 1.72 (s, 4H, 2CH$_2$), 2.29 (m, 2H, CH$_2$), 2.58 (s, 2H, CH$_2$), 3.69 (s, 3H, OCH$_3$), 5.33 (s, 1H, CH of pyran), 5.64 (s, 2H, NH$_2$; D$_2$O exchangeable), 6.72 (d, J = 8.4 Hz, 2H, ArH), 6.75 (d, J = 2.1 Hz, 1H, ArH), 6.82 (d, J = 1.9 Hz, 1H, ArH), 6.92 (s, 1H, ArH), 7.15 (t, J = 7.9 Hz, 1H, ArH), 7.24 (d, J = 8.5 Hz, 1H, ArH), 7.51 (t, J = 8.7 Hz, 2H, ArH), 7.97 (dd, J = 4.9, 8.5 Hz, 2H, ArH); ^{13}C NMR (100 MHz, DMSO-d_6): δ = 22.55, 22.78, 23.44, 32.51, 39.00, 55.43, 98.05, 110.73, 111.70, 112.99, 114.27, 117.49, 117.81, 119.77, 125.25, 130.33, 130.67, 130.96, 132.07, 132.17, 146.86, 148.31, 151.58, 151.97, 153.10, 155.29, 159.72, 164.81, 167.35; elemental analysis for C$_{29}$H$_{25}$N$_2$O$_5$FS, calcd: C, 65.40; H, 4.73; N, 5.26; found: C, 65.42; H, 4.64; N, 5.30.

5.1.3.3. Characterization of 11-Amino-12-(3-nitrophenyl)-7,9,10,12-tetrahydro-8H-chromeno[2, 3-b]quinolin-3-yl-4-fluorobenzenesulfonate (4c). Yield = 74%, mp = 260−265 °C, yellow solid, IR (KBr, v, cm^{-1}): 1350 (S=O), 3398 and 3480 (NH$_2$); ^{1}H NMR (400 MHz, DMSO-d_6): δ = 1.71 (s, 4H, 2CH$_2$), 2.28 (m, 2H, CH$_2$), 2.59 (s, 2H, CH$_2$), 5.63 (s, 1H, CH of pyran), 5.84 (s, 2H, NH$_2$; D$_2$O exchangeable), 6.78 (dd, J = 2.1, 8.5 Hz, 1H, ArH), 6.89 (d, J = 1.9 Hz, 1H, ArH), 7.28 (d, J = 8.5 Hz, 1H, ArH), 7.52 (m, 2H, ArH), 7.59 (t, J = 7.2 Hz, 2H, ArH), 7.97 (dd, J = 4.9, 8.5 Hz, 2H, ArH), 8.04 (d, J = 7.8 Hz, 1H, ArH), 8.28 (s, 1H, ArH); ^{13}C NMR (100 MHz, DMSO-d_6): δ = 22.49, 22.72, 23.45, 32.51, 38.49, 97.42, 111.08, 113.23, 117.58, 117.81, 117.89, 122.13, 122.38, 124.30, 130.80, 130.91, 132.10, 132.20, 134.33, 147.33, 148.21, 148.63, 151.71, 152.07, 153.59, 155.24, 164.83, 167.36; HRMS (m/z): [M + H]$^+$ calcd for C$_{28}$H$_{22}$N$_3$O$_6$FS: 548.1286; found: 548.12743; elemental analysis for C$_{28}$H$_{22}$N$_3$O$_6$FS, calcd: C, 61.42; H, 4.05; N, 7.67; found: C, 61.442; H, 4.00; N, 7.69.

5.1.3.4. Characterization of 11-Amino-12-(3,4-dichlorophenyl)-7,9,10,12-tetrahydro-8H-chromeno[2, 3-b]quinolin-3-yl-4-fluorobenzenesulfonate (4d). Yield = 95%, mp = 255−260 °C, yellow solid, IR (KBr, v, cm^{-1}): 1376 (S=O), 3304 and 3492 (NH$_2$); ^{1}H NMR (400 MHz, DMSO-d_6): δ = 1.72 (s, 4H, 2CH$_2$), 2.29 (m, 2H, CH$_2$), 2.59 (s, 2H, CH$_2$), 5.44 (s, 1H, CH of pyran), 5.78 (s, 2H, NH$_2$; D$_2$O exchangeable), 6.77 (dd, J = 2.3, 8.4 Hz, 1H, ArH), 6.86 (d, J = 2.6 Hz, 1H, ArH), 7.08 (dd, J = 1.8, 8.4 Hz, 1H, ArH), 7.28 (d, J = 8.5 Hz, 1H, ArH), 7.52 (t, J = 8.5 Hz, 3H, ArH), 7.56 (d, J = 1.8 Hz, 1H, ArH), 7.97 (dd, J = 5.0, 8.8 Hz, 2H, ArH); ^{13}C NMR (100 MHz, DMSO-d_6): δ = 22.49, 22.72, 23.45, 32.50, 38.09, 97.23, 111.01, 113.18, 117.59, 117.82, 124.22, 127.92, 129.56, 129.88, 130.77, 130.84, 131.40, 131.59, 132.10, 132.20, 146.18, 148.58, 151.57, 152.02, 153.52, 155.16, 164.82, 167.36; MS (EI) m/z (C$_{28}$H$_{21}$N$_2$O$_4$Cl$_2$SF): 575.59 (M$^+$+4, 20.26%), 573.11 (M$^+$ + 1, 16.54%), 571.87 (M$^+$, 11.67%), 396.39 (100%); elemental analysis for C$_{28}$H$_{21}$N$_2$O$_4$Cl$_2$FS, calcd: C, 58.85; H, 3.70; N, 4.90; found: C, 58.86; H, 3.72; N, 4.88.

4.1.3.5. Characterization of 11-Amino-12-(2-methoxyphenyl)-7,9,10,12-tetrahydro-8H-chromeno[2, 3-b]quinolin-3-yl-4-fluorobenzenesulfonate (4e). Yield = 74%, mp = 105−110 °C, yellow solid, IR (KBr, v, cm^{-1}): 1380 (S=O), 3330 and 3484 (NH$_2$); ^{1}H NMR (400 MHz, DMSO-d_6): δ = 1.70 (s, 4H, 2CH$_2$), 2.29 (m, 2H, CH$_2$), 2.57 (s, 2H, CH$_2$), 3.81 (s, 3H, OCH$_3$), 5.33 (s, 2H, NH$_2$; D$_2$O exchangeable), 5.51 (s, 1H, CH of pyran), 6.70 (dd, J = 2.4, 8.5 Hz, 1H, ArH), 6.78 (d, J = 2.4 Hz, 1H, ArH), 6.83 (t, J = 7.6 Hz, 1H, ArH), 7.00 (t, J = 8.5 Hz, 2H, ArH), 7.11 (d, J = 8.6 Hz, 1H, ArH), 7.17 (m, 1H, ArH), 7.52 (t, J = 8.8 Hz, 2H, ArH), 7.97 (dd, J = 5.0, 8.9 Hz, 2H, ArH); ^{13}C NMR (100 MHz, DMSO-d_6): δ = 22.53, 22.77, 23.35, 32.43, 33.13, 56.35, 97.89, 110.35, 112.27, 112.82, 117.56, 117.79, 121.76, 124.56, 128.70, 129.65, 130.77, 130.84, 132.11, 132.21, 133.09, 148.21, 151.72, 151.84, 152.82, 155.15, 155.87, 164.80, 167.34; elemental analysis for C$_{29}$H$_{25}$N$_2$O$_5$FS, calcd: C, 65.40; H, 4.73; N, 5.26; found: C, 65.37; H, 4.66; N, 5.20.

5.1.3.6. Characterization of 11-Amino-12-(3-bromophenyl)-7,9,10,12-tetrahydro-8H-chromeno[2, 3-b]quinolin-3-yl-4-methoxybenzenesulfonate (4f). Yield = 90%, mp = 105−110 °C, yellow solid, IR (KBr, v, cm^{-1}): 1376 (S=O), 3369 and 3477 (NH$_2$); ^{1}H NMR (400 MHz, DMSO-d_6): δ = 1.72 (s, 4H, 2CH$_2$), 2.29 (m, 2H, CH$_2$), 2.59 (s, 2H, CH$_2$), 3.87 (s, 3H, OCH$_3$), 5.41 (s, 1H, CH of pyran), 5.74 (s, 2H, NH$_2$; D$_2$O exchangeable), 6.75 (dd, J = 2.3, 8.3, 1H, ArH), 6.80 (d, J = 2.2 Hz, 1H, ArH), 7.16 (d, J = 8.8 Hz, 3H, ArH), 7.20 (m, 2H, ArH), 7.36 (d, J = 7.7 Hz, 1H, ArH), 7.54 (s, 1H, ArH), 7.79 (d, J = 8.9 Hz, 2H, ArH); ^{13}C NMR (100 MHz, DMSO-d_6): δ = 22.51, 22.73, 23.46, 32.58, 38.56, 56.43, 97.65, 110.86, 113.10, 115.45, 117.82, 122.25, 124.46, 125.76, 126.70, 130.09, 130.26, 130.61, 131.14, 131.52, 148.02, 148.71, 151.53, 151.98, 153.35, 155.26, 164.55; HRMS (m/z): [M + H]$^+$ calcd for C$_{29}$H$_{25}$N$_2$O$_5$SBr: 593.0740; found: 593.0721; elemental analysis for C$_{29}$H$_{25}$N$_2$O$_5$SBr, calcd: C, 58.69; H, 4.25; N, 4.72; found: C, 58.73; H, 4.21; N, 4.69.

5.1.3.7. Characterization of 11-Amino-12-(3-methoxyphenyl)-7,9,10,12-tetrahydro-8H-chromeno[2, 3-b]quinolin-3-yl-4-methoxybenzenesulfonate (4g). Yield = 88%, mp = 195−200 °C, yellow solid, IR (KBr, v, cm^{-1}): 1376 (S=O), 3388 and 3491 (NH$_2$); ^{1}H NMR (400 MHz, DMSO-d_6): δ = 1.72 (s, 4H, 2CH$_2$), 2.29 (m, 2H, CH$_2$), 2.58 (s, 2H, CH$_2$), 3.69 (s, 3H, OCH$_3$), 3.87 (s, 3H, OCH$_3$), 5.33 (s, 1H, CH of pyran), 5.63 (s, 2H, NH$_2$; D$_2$O exchangeable), 6.72 (m, 2H, ArH), 6.76 (s, 2H, ArH), 6.92 (s, 1H, ArH), 7.13 (s, 1H, ArH), 7.16 (d, J = 9.1 Hz, 2H, ArH), 7.23 (d, J = 8.4 Hz, 1H, ArH), 7.80 (d, J = 8.8 Hz, 2H, ArH); ^{13}C NMR (100 MHz, DMSO-d_6): δ = 22.55, 22.78, 23.45, 32.50, 38.97, 55.42, 56.41, 98.07, 110.66, 111.66, 112.94, 114.27, 115.44, 117.58, 119.77,

124.98, 125.82, 130.32, 130.56, 131.13, 146.91, 148.52, 151.47, 151.97, 153.06, 155.30, 159.69, 164.53; MS (EI) m/z ($C_{30}H_{28}N_2O_6S$): 545.03 ($M^+ + 1$, 1.73%), 544.06 (M^+, 2.02%), 141.25 (100%); elemental analysis for $C_{30}H_{28}N_2O_6S$, calcd: C, 66.16; H, 5.18; N, 5.14; found: C, 66.09; H, 5.23; N, 5.17.

5.1.3.8. Characterization of 11-Amino-12-(3-nitrophenyl)-7,9,10,12-tetrahydro-8H-chromeno[2, 3-b]quinolin-3-yl-4-methoxybenzenesulfonate (4h). Yield = 77%, mp = 242−247 °C, yellow solid, IR (KBr, v, cm^{-1}): 1375 (S=O), 3339 and 3454 (NH$_2$); ^{1}H NMR (400 MHz, DMSO-d_6): δ = 1.71 (s, 4H, 2CH$_2$), 2.28 (m, 2H, CH$_2$), 2.59 (s, 2H, CH$_2$), 3.87 (s, 3H, OCH$_3$), 5.63 (s, 1H, CH of pyran), 5.84 (s, 2H, NH$_2$; D$_2$O exchangeable), 6.77 (dd, J = 1.8, 8.3, 1H, ArH), 6.83 (d, J = 1.9 Hz, 1H, ArH), 7.15 (d, J = 8.8 Hz, 2H, ArH), 7.27 (d, J = 8.5 Hz, 1H, ArH), 7.57 (m, 2H, ArH), 7.79 (d, J = 8.8 Hz, 2H, ArH), 8.04 (d, J = 7.8 Hz, 1H, ArH), 8.28 (s, 1H, ArH). ^{13}C NMR (100 MHz, DMSO-d_6): δ = 22.49, 22.72, 23.46, 32.51, 38.49, 56.41, 97.46, 110.99, 113.20, 115.44, 117.96, 122.13, 122.36, 124.03, 125.73, 130.68, 130.90, 131.14, 134.34, 147.38, 148.21, 148.86, 151.62, 152.07, 153.57, 155.26, 164.56; elemental analysis for $C_{29}H_{25}N_3O_7S$, calcd: C, 62.25; H, 4.50; N, 7.51; found: C, 62.22; H, 4.56; N, 7.53.

5.1.3.9. Characterization of 11-Amino-12-(3,4-dichloro-phenyl)-7,9,10,12-tetrahydro-8H-chromeno[2, 3-b]quinolin-3-yl-4-methoxybenzenesulfonate (4i). Yield = 93%, mp = 101−106 °C, yellow solid, IR (KBr, v, cm^{-1}): 1376 (S=O), 3370 and 3468 (NH$_2$); ^{1}H NMR (400 MHz, DMSO-d_6): δ = 1.72 (s, 4H, 2CH$_2$), 2.29 (m, 2H, CH$_2$), 2.58 (s, 2H, CH$_2$), 3.87 (s, 3H, OCH$_3$), 5.43 (s, 1H, CH of pyran), 5.78 (s, 2H, NH$_2$; D$_2$O exchangeable), 6.75 (dd, J = 2.2, 8.4, 1H, ArH), 6.81 (d, J = 2.2 Hz, 1H, ArH), 7.08 (dd, J = 1.7, 8.4 Hz, 1H, ArH), 7.16 (d, J = 8.9 Hz, 2H, ArH), 7.26 (d, J = 8.5 Hz, 1H, ArH), 7.51 (d, J = 8.4 Hz, 1H, ArH), 7.65 (d, J = 1.7 Hz, 1H, ArH), 7.80 (d, J = 8.9 Hz, 2H, ArH); ^{13}C NMR (100 MHz, DMSO-d_6): 22.45, 22.66, 23.39, 32.41, 38.10, 56.39, 97.26, 110.89, 113.21, 115.44, 117.90, 123.91, 125.68, 127.87, 129.46, 129.93, 130.66, 131.13, 131.46, 131.55, 146.12, 148.78, 151.42, 152.02, 153.56, 155.16, 164.56; elemental analysis for $C_{29}H_{24}N_2O_5SCl_2$, calcd: C, 59.70; H, 4.15; N, 4.80; found: C, 59.69; H, 4.10; N, 4.78.

5.1.3.10. Characterization of 11-Amino-12-(2-methoxy-phenyl)-7,9,10,12-tetrahydro-8H-chromeno[2, 3-b]quinolin-3-yl-4-methoxybenzenesulfonate (4j). Yield = 78%, mp = 100−105 °C, yellow solid, IR (KBr, v, cm^{-1}): 1376 (S=O), 3387 and 3479 (NH$_2$); ^{1}H NMR (400 MHz, DMSO-d_6): δ = 1.70 (s, 4H, 2CH$_2$), 2.26 (m, 2H, CH$_2$), 2.57 (s, 2H, CH$_2$), 3.81 (s, 3H, OCH$_3$), 3.85 (s, 3H, OCH$_3$), 5.32 (s, 2H, NH$_2$; D$_2$O exchangeable), 5.50 (s, 1H, CH of pyran), 6.75 (dd, J = 2.2, 8.4, 1H, ArH), 6.72 (s, 1H, ArH), 6.84 (t, J = 7.4 Hz, 1H, ArH), 7.00 (t, J = 8.1 Hz, 2H, ArH), 7.09 (d, J = 8.4 Hz, 1H, ArH), 7.16 (d, J = 8.7 Hz, 3H, ArH), 7.79 (d, J = 1.7 Hz, 2H, ArH); ^{13}C NMR (100 MHz, DMSO-d_6): 22.52, 22.77, 23.33, 32.42, 33.10, 56.37, 56.41, 97.95, 110.27, 112.28, 112.76, 115.42, 117.38, 121.77, 124.29, 125.79, 128.68, 129.64, 130.65, 131.14, 133.15, 148.43, 151.76, 152.84, 155.18, 155.85, 164.52; elemental analysis for $C_{30}H_{28}N_2O_6S$, calcd: C, 66.16; H, 5.18; N, 5.14; found: C, 66.20; H, 5.18; N, 5.09.

5.1.3.11. Characterization of 11-Amino-12-(3-bromo-phenyl)-7,9,10,12-tetrahydro-8H-chromeno[2, 3-b]quinolin-3-yl-4-methylbenzenesulfonate (4k). Yield = 86%, mp = 127−132 °C, yellow solid, IR (KBr, v, cm^{-1}): 1374 (S=O), 3379 and 3483 (NH$_2$); ^{1}H NMR (400 MHz, DMSO-d_6): δ =

1.71 (s, 4H, 2CH$_2$), 2.29 (m, 2H, CH$_2$), 2.43 (s, 3H, CH$_3$), 2.58 (s, 2H, CH$_2$), 5.40 (s, 1H, CH of pyran), 5.75 (s, 2H, NH$_2$; D$_2$O exchangeable), 6.77 (d, J = 8.37 Hz, 1H, ArH), 6.80 (s, 1H, ArH), 7.17 (t, J = 8.7 Hz, 1H, ArH), 7.23 (t, J = 8.7 Hz, 2H, ArH), 7.36 (d, J = 7.6 Hz, 1H, ArH), 7.47 (d, J = 7.9 Hz, 2H, ArH), 7.52 (s, 1H, ArH), 7.76 (d, J = 8.0 Hz, 2H, ArH); ^{13}C NMR (100 MHz, DMSO-d_6): 21.67, 22.75, 23.45, 31.28, 36.27, 38.59, 97.99, 110.80, 113.14, 117.77, 122.29, 124.54, 126.70, 128.73, 130.13, 130.26, 130.77, 131.53, 131.74, 146.46, 148.00, 148.68, 151.54, 152.01, 153.40, 155.24, 162.85; elemental analysis for $C_{29}H_{25}N_2O_4SBr$, calcd: C, 60.32; H, 4.36; N, 4.85; found: C, 60.29; H, 4.30; N, 4.89.

5.1.3.12. Characterization of 11-Amino-12-(3-methoxy-phenyl)-7,9,10,12-tetrahydro-8H-chromeno[2, 3-b]quinolin-3-yl-4-methylbenzenesulfonate (4l). Yield = 89%, mp = 120−125 °C, yellow solid, IR (KBr, v, cm^{-1}): 1375 (S=O), 3359 and 3467 (NH$_2$); ^{1}H NMR (400 MHz, DMSO-d_6): δ = 1.71 (s, 4H, 2CH$_2$), 2.28 (m, 2H, CH$_2$), 2.43 (s, 3H, CH$_3$), 2.58 (s, 2H, CH$_2$), 3.69 (s, 3H, OCH$_3$), 5.32 (s, 1H, CH of pyran), 5.65 (s, 2H, NH$_2$; D$_2$O exchangeable), 6.72 (m, 2H, ArH), 6.75 (s, 2H, ArH), 7.92 (s, 1H, ArH), 7.15 (t, J = 7.9 Hz, 1H, ArH), 7.23 (d, J = 8.1 Hz, 1H, ArH), 7.47 (d, J = 8.1 Hz, 2H, ArH), 7.76 (d, J = 8.3 Hz, 2H, ArH); ^{13}C NMR (100 MHz, DMSO-d_6): 21.66, 22.55, 22.78, 23.44, 32.50, 38.97, 55.42, 98.04, 110.59, 111.67, 112.96, 114.27, 117.52, 119.77, 125.04, 128.70, 130.32, 130.60, 130.75, 131.79, 146.39, 146.89, 148.46, 151.47, 151.97, 153.06, 155.28, 159.70; HRMS (m/z): [M + H]$^+$ calcd for $C_{30}H_{28}N_2O_5S$: 529.1792; found: 529.17834; elemental analysis for $C_{30}H_{28}N_2O_5S$, calcd: C, 68.16; H, 5.34; N, 5.30; found: C, 68.10; H, 5.37; N, 5.28.

5.1.3.13. Characterization of 11-Amino-12-(3-nitrophen-yl)-7,9,10,12-tetrahydro-8H-chromeno[2, 3-b]quinolin-3-yl-4-methylbenzenesulfonate (4m). Yield = 71%, mp = 109−114 °C, yellow solid; ^{1}H NMR (400 MHz, DMSO-d_6): δ = 1.71 (s, 4H, 2CH$_2$), 2.26 (m, 2H, CH$_2$), 2.42 (s, 3H, CH$_3$), 2.58 (s, 2H, CH$_2$), 5.67 (s, 1H, CH of pyran), 5.88 (s, 2H, NH$_2$; D$_2$O exchangeable), 6.77 (dd, J = 1.9, 8.4, 1H, ArH), 6.83 (d, J = 1.9 Hz, 1H, ArH), 7.27 (d, J = 8.5 Hz, 1H, ArH), 7.46 (d, J = 8.0 Hz, 2H, ArH), 7.55 (t, J = 7.9 Hz, 1H, ArH), 7.62 (d, J = 7.6 Hz, 1H, ArH), 7.75 (d, J = 8.1 Hz, 2H, ArH), 8.03 (d, J = 7.8 Hz, 1H, ArH), 8.27 (s, 1H, ArH); ^{13}C NMR (100 MHz, DMSO-d_6): 21.64, 22.47, 22.69, 23.42, 32.46, 38.44, 97.45, 110.90, 113.25, 117.90, 122.07, 122.37, 124.12, 128.69, 130.74, 130.88, 131.64, 134.33, 146.47, 147.33, 148.23, 148.77, 151.59, 152.11, 153.58, 155.25; elemental analysis for $C_{29}H_{25}N_3O_6S$, calcd: C, 64.08; H, 4.64; N, 7.73; found: C, 64.11; H, 4.71; N, 7.68.

5.1.3.14. Characterization of 11-Amino-12-(3,4-dichlor-ophenyl)-7,9,10,12-tetrahydro-8H-chromeno[2, 3-b]-quinolin-3-yl-4-methylbenzenesulfonate (4n). Yield = 96%, mp = 130−135 °C, yellow solid, IR (KBr, v, cm^{-1}): 1365 (S=O), 3373 and 3468 (NH$_2$); ^{1}H NMR (400 MHz, DMSO-d_6): δ = 1.71 (s, 4H, 2CH$_2$), 2.26 (m, 2H, CH$_2$), 2.42 (s, 3H, CH$_3$), 2.58 (s, 2H, CH$_2$), 5.43 (s, 1H, CH of pyran), 5.78 (s, 2H, NH$_2$; D$_2$O exchangeable), 6.76 (dd, J = 2.3, 8.4 Hz, 1H, ArH), 6.81 (d, J = 2.2 Hz,1H, ArH), 7.08 (dd, J = 1.8, 8.4 Hz, 1H, ArH), 7.26 (d, J = 8.5 Hz, 1H, ArH), 7.47 (d, J = 8.2 Hz, 2H, ArH), 7.51 (d, J = 8.4 Hz, 1H, ArH), 7.64 (d, J = 1.8 Hz, 1H, ArH), 7.76 (d, J = 8.2 Hz, 2H, ArH); ^{13}C NMR (100 MHz, DMSO-d_6): 21.66, 22.49, 22.73, 23.45, 32.51, 38.10, 97.25, 110.85, 113.17, 117.82, 124.02, 127.93, 128.72, 129.56, 129.92, 130.70, 130.75, 131.40, 131.58, 131.73, 146.22, 146.42, 148.77, 151.49, 152.03, 153.51, 155.16; MS (EI) m/z

($C_{29}H_{24}N_2O_4SCl_2$): 569.18 (M^+ + 2, 23.89%), 567.98 (M^+, 95.14%), 170.78 (100%); elemental analysis for $C_{29}H_{24}N_2O_4SCl_2$, calcd: C, 61.38; H, 4.26; N, 4.94; found: C, 61.40; H, 4.32; N, 4.99.

5.1.3.15. Characterization of 11-Amino-12-(2-methoxyphenyl)-7,9,10,12-tetrahydro-8H-chromeno[2, 3-b]quinolin-3-yl-4-methylbenzenesulfonate (4o). Yield = 70%, mp = 105−110 °C, yellow solid, IR (KBr, v, cm^{-1}): 1372 (S=O), 3409 and 3504 (NH$_2$); ^{1}H NMR (400 MHz, DMSO-d_6): δ = 1.70 (s, 4H, 2CH$_2$), 2.26 (m, 2H, CH$_2$), 2.42 (s, 3H, CH$_3$), 2.56 (s, 2H, CH$_2$), 3.80 (s, 3H, OCH$_3$), 5.33 (s, 2H, NH$_2$; D$_2$O exchangeable), 5.50 (s, 1H, CH of pyran), 6.69 (d, J = 2.2 Hz, 1H, ArH), 6.72 (s, 1H, ArH), 6.84 (t, J = 7.4 Hz, 1H, ArH), 7.00 (t, J = 7.9 Hz, 2H, ArH), 7.10 (d, J = 8.3 Hz, 1H, ArH), 7.17 (t, J = 7.7 Hz, 1H, ArH), 7.47 (d, J = 8.2 Hz, 2H, ArH), 7.75 (d, J = 8.2 Hz, 2H, ArH); ^{13}C NMR (100 MHz, DMSO-d_6): 21.65, 22.53, 22.77, 23.34, 32.43, 33.11, 56.36, 97.93, 110.20, 112.28, 112.80, 117.33, 121.76, 124.35, 128.68, 128.72, 129.64, 130.71, 131.75, 133.13, 146.36, 148.38, 151.71, 151.76, 152.82, 155.16, 155.86; elemental analysis for $C_{30}H_{28}N_2O_5S$, calcd: C, 68.16; H, 5.34; N, 5.30; found: C, 68.08; H, 5.41; N, 5.28.

5.1.3.16. Characterization of 11-Amino-12-(3-bromophenyl)-7,9,10,12-tetrahydro-8H-chromeno[2, 3-b]quinolin-3-yl-benzenesulfonate (4p). Yield = 89%, mp = 100−105 °C, yellow solid, IR (KBr, v, cm^{-1}): 1376 (S=O), 3399 and 3482 (NH$_2$); ^{1}H NMR (400 MHz, DMSO-d_6): δ = 1.72 (s, 4H, 2CH$_2$), 2.29 (m, 2H, CH$_2$), 2.58 (s, 2H, CH$_2$), 5.41 (s, 1H, CH of pyran), 5.74 (s, 2H, NH$_2$; D$_2$O exchangeable), 6.78 (d, J = 10.6 Hz, 2H, ArH), 7.17 (t, J = 9.1 Hz, 1H, ArH), 7.23 (t, J = 7.6 Hz, 2H, ArH), 7.36 (d, J = 7.4 Hz, 1H, ArH), 7.54 (s, 1H, ArH), 7.68 (t, J = 7.7 Hz, 2H, ArH), 7.84 (t, J = 7.1 Hz, 1H, ArH), 7.88 (d, J = 7.7 Hz, 2H, ArH); ^{13}C NMR (100 MHz, DMSO-d_6): 22.51, 22.73, 23.45, 32.50, 38.56, 97.63, 110.85, 113.12, 117.76, 122.26, 124.62, 126.69, 128.71, 130.10, 130.25, 130.32, 130.66, 131.51, 134.57, 135.66, 147.97, 148.57, 151.56, 151.98, 153.36, 155.2; elemental analysis for $C_{28}H_{23}N_2O_4SBr$, calcd: C, 59.69; H, 4.11; N, 4.97; found: C, 59.77; H, 4.07; N, 4.99.

5.1.3.17. Characterization of 11-Amino-12-(3-methoxyphenyl)-7,9,10,12-tetrahydro-8H-chromeno[2, 3-b]quinolin-3-yl-benzenesulfonate (4q). Yield = 86%, mp = 220−225 °C, yellow solid, IR (KBr, v, cm^{-1}): 1371 (S=O), 3323 and 3473 (NH$_2$); ^{1}H NMR (400 MHz, DMSO-d_6): δ = 1.71 (s, 4H, 2CH$_2$), 2.28 (m, 2H, CH$_2$), 2.58 (s, 2H, CH$_2$), 3.69 (s, 3H, OCH$_3$), 5.32 (s, 1H, CH of pyran), 5.63 (s, 2H, NH$_2$; D$_2$O exchangeable), 6.72 (m, 2H, ArH), 6.76 (s, 2H, ArH), 6.92 (s,1H, ArH), 7.14 (t, J = 7.93 Hz, 1H, ArH), 7.23 (d, J = 8.9 Hz, 1H, ArH), 7.68 (t, J = 7.6 Hz, 2H, ArH), 7.83 (t, J = 7.4 Hz, 1H, ArH), 7.89 (d, J = 7.7 Hz, 2H, ArH); ^{13}C NMR (100 MHz, DMSO-d_6): 22.55, 22.78, 23.45, 32.50, 38.97, 98.05, 110.65, 111.69, 112.97, 114.26, 117.53, 119.77, 125.14, 128.70, 130.33, 130.62, 134.65, 135.63, 146.88, 148.38, 151.50, 151.97, 153.08, 155.27, 159.71; elemental analysis for $C_{29}H_{26}N_2O_5S$, calcd: C, 67.69; H, 5.09; N, 5.44; found: C, 67.72; H, 5.10; N, 5.50.

5.1.3.18. Characterization of 11-Amino-12-(3-nitrophenyl)-7,9,10,12-tetrahydro-8H-chromeno[2, 3-b]quinolin-3-yl-benzenesulfonate (4r). Yield = 72%, mp = 210−215 °C, yellow solid; ^{1}H NMR (400 MHz, DMSO-d_6): δ = 1.71 (s, 4H, 2CH$_2$), 2.28 (m, 2H, CH$_2$), 2.59 (s, 2H, CH$_2$), 5.63 (s, 1H, CH of pyran), 5.84 (s, 2H, NH$_2$; D$_2$O exchangeable), 6.78 (dd, J = 2.1, 8.4 Hz, 1H, ArH), 6.82 (d, J = 2.1 Hz, 1H, ArH), 6.85 (d, J = 8.9 Hz, 1H, ArH), 7.12 (m, 1H, ArH), 7.27 (d, J = 8.4 Hz, 1H, ArH), 7.54 (d, J = 7.7 Hz, 1H, ArH), 7.58 (m, 1H, ArH), 7.67 (t, J = 7.7 Hz, 1H, ArH), 7.84 (t, J = 7.9 Hz, 1H, ArH), 7.88 (d, J = 7.7 Hz, 1H, ArH), 8.04 (d, J = 7.6 Hz, 1H, ArH), 8.28 (s, 1H, ArH); ^{13}C NMR (100 MHz, DMSO-d_6): 22.49, 22.72, 29.50, 32.52, 38.48, 97.43, 110.99, 113.21, 117.88, 122.14, 122.37, 124.19, 128.70, 130.32, 130.73, 130.91, 134.34, 134.57, 135.66, 147.36, 148.20, 148.71, 151.66, 152.06, 153.57, 155.22; elemental analysis for $C_{28}H_{23}N_3O_6S$, calcd: C, 63.51; H, 4.38; N, 7.93; found: C, 63.44; H, 4.43; N, 7.89.

5.1.3.19. Characterization of 11-Amino-12-(3,4-dichlorophenyl)-7,9,10,12-tetrahydro-8H-chromeno[2, 3-b]quinolin-3-yl-benzenesulfonate (4s). Yield = 92%, mp = 215−220 °C, yellow solid, IR (KBr, v, cm^{-1}): 1369 (S=O), 3368 and 3463 (NH$_2$); ^{1}H NMR (400 MHz, DMSO-d_6): δ = 1.72 (s, 4H, 2CH$_2$), 2.29 (m, 2H, CH$_2$), 2.58 (s, 2H, CH$_2$), 5.43 (s, 1H, CH of pyran), 5.77 (s, 2H, NH$_2$; D$_2$O exchangeable), 6.78 (d, J = 13.0 Hz, 1H, ArH), 7.08 (d, J = 7.8 Hz, 1H, ArH), 7.17 (m, 2H, ArH), 7.27 (d, J = 7.8, 2H, ArH), 7.51 (d, J = 8.1 Hz, 1H, ArH), 7.67 (m, 2H, ArH), 7.83 (d, J = 6.9 Hz, 1H, ArH), 7.89 (d, J = 7.3 Hz, 1H, ArH); ^{13}C NMR (100 MHz, DMSO-d_6): 22.49, 22.72, 23.44, 32.50, 38.08, 97.36, 110.92, 113.12, 117.83, 123.93, 127.92, 128.71, 129.56, 129.88, 130.33, 130.71, 131.37, 131.99, 134.58, 135.67, 146.25, 148.51, 151.58, 152.02, 153.40, 155.24; elemental analysis for $C_{28}H_{22}N_2O_4SCl_2$, calcd: C, 60.77; H, 4.01; N, 5.06; found: C, 60.65; H, 4.17; N, 5.15.

5.1.3.20. Characterization of 11-Amino-12-(2-methoxyphenyl)-7,9,10,12-tetrahydro-8H-chromeno[2, 3-b]quinolin-3-yl-benzenesulfonate (4t). Yield = 79%, mp = 103−108 °C, yellow solid, IR (KBr, v, cm^{-1}): 1379 (S=O), 3363 and 3489 (NH$_2$); ^{1}H NMR (400 MHz, DMSO-d_6): δ = 1.70 (s, 4H, 2CH$_2$), 2.25 (m, 2H, CH$_2$), 2.56 (s, 2H, CH$_2$), 3.80 (s, 3H, OCH$_3$), 5.33 (s, 2H, NH$_2$; D$_2$O exchangeable), 5.49 (s, 1H, CH of pyran), 6.69 (d, J = 2.4 Hz, 1H, ArH), 6.71 (s, 1H, ArH), 6.84 (t, J = 7.2 Hz, 1H, ArH), 7.00 (t, J = 7.8 Hz, 2H, ArH), 7.10 (d, J = 9.1 Hz, 1H, ArH), 7.17 (m, 1H, ArH), 7.67 (t, J = 7.8 Hz, 2H, ArH), 7.83 (t, J = 7.5 Hz, 1H, ArH), 7.88 (d, J = 7.3 Hz, 2H, ArH); ^{13}C NMR (100 MHz, DMSO-d_6): 22.53, 22.77, 23.34, 32.43, 33.12, 56.37, 97.92, 110.25, 112.29, 112.81, 117.30, 121.77, 124.45, 128.71, 129.63, 130.29, 130.70, 133.12, 134.60, 135.61, 148.29, 151.70, 151.79, 152.84, 155.15, 155.86; MS (EI) m/z ($C_{29}H_{26}N_2O_5S$,): 515.30 (M^+ + 1, 3.13%), 514.25 (M^+, 7.03%), 161.35 (100%); HRMS (m/z): $[M + H]^+$ calcd for $C_{29}H_{26}N_2O_5S$: 515.1635; found: 515.16263; elemental analysis for $C_{29}H_{26}N_2O_5S$, calcd: C, 67.69; H, 5.09; N, 5.44; found: C, 67.68; H, 5.05; N, 5.36.

5.1.4. General Procedure for the Preparation of 2-[11-Amino-12-(substituated)-7,9,10,12-tetrahydro-8H-chromeno[2,3-b]quinolin-3-yl]oxy-1-substituted-phenylethan-1-one (5a−j). In a 50 mL round-bottom flask, a mixture of compounds 3a−e (1 mmol), bromoacetophenone derivatives (1 mmol), and K$_2$CO$_3$ (2 mmol, 0.27 g) was added into acetone (10 mL) and refluxed for 3−5 h. The reaction was monitored by TLC, and after completion of the reaction, the solvent was evaporated under vacuum. The precipitate was purified by column chromatography on silica gel (petroleum ether/ethyl acetate = 5:1, then 3:1, and then 1:1, v/v) to afford the title compounds 5a−j.

5.1.4.1. Characterization of 2-[11-Amino-12-(3-bromophenyl)-7,9,10,12-tetrahydro-8H-chromeno[2, 3-b]quinolin-3-yl]oxy-1-(4-chlorophenyl)ethan-1-one (5a). Yield = 86%, mp = 107−112 °C, yellow solid; ^{1}H NMR (400 MHz, DMSO-

d_6): δ = 1.72 (s, 4H, 2CH$_2$), 2.30 (m, 2H, CH$_2$), 2.59 (s, 2H, CH$_2$), 5.34 (s, 1H, CH of pyran), 5.58 (s, 2H, COCH$_2$O), 5.67 (s, 2H, NH$_2$; D$_2$O exchangeable), 6.69 (d, J = 8.3 Hz, 1H, ArH), 6.78 (d, J = 1.7 Hz, 1H, ArH), 7.11 (d, J = 8.4 Hz, 1H, ArH), 7.17 (m, 2H, ArH), 7.28 (t, J = 7.7 Hz, 1H, ArH), 7.34 (d, J = 3.0 Hz 1H, ArH), 7.54 (s, 1H, ArH), 7.66 (d, J = 8.3 Hz, 2H, ArH), 8.05 (d, J = 8.3 Hz, 1H, ArH); elemental analysis for C$_{30}$H$_{24}$N$_2$O$_3$ClBr, calcd: C, 62.57; H, 4.20; N, 4.86; found: C, 62.59; H, 4.16; N, 4.94.

5.1.4.2. Characterization of 2-[11-Amino-12-(3-methoxyphenyl)-7,9,10,12-tetrahydro-8H-chromeno[2, 3-b]-quinolin-3-yl]oxy-1-(4-chlorophenyl)ethan-1-one (5b). Yield = 87%, mp = 103−108 °C, yellow solid; ^{1}H NMR (400 MHz, DMSO-d_6): δ = 1.71 (s, 4H, 2CH$_2$), 2.29 (m, 2H, CH$_2$), 2.58 (s, 2H, CH$_2$), 3.70 (s, 3H, OCH$_3$), 5.25 (s, 1H, CH of pyran), 5.75 (br. S, 2H, NH$_2$; D$_2$O exchangeable and 2H, COCH$_2$O), 6.71 (m, 4H, ArH), 6.94 (s, 1H, ArH), 7.12 (m, 2H, ArH), 7.66 (d, J = 7.1 Hz, 2H, ArH), 8.05 (d, J = 6.24 Hz, 2H, ArH); ^{13}C NMR (100 MHz, DMSO-d_6): 21.97, 22.36, 32.20, 35.82, 38.91, 55.54, 70.45, 98.45, 102.91, 103.79, 109.34, 111.32, 112.57, 114.26, 119.82, 129.47, 129.90, 130.16, 130.33, 133.51, 139.17, 140.92, 147.80, 151.73, 151.86, 152.83, 157.87, 194.27; elemental analysis for C$_{31}$H$_{27}$N$_2$O$_4$Cl, calcd: C, 70.65; H, 5.16; N, 5.32; found: C, 70.59; H, 5.06; N, 5.28.

5.1.4.3. Characterization of 2-[11-Amino-12-(3-nitrophenyl)-7,9,10,12-tetrahydro-8H-chromeno[2, 3-b]quinolin-3-yl]oxy-1-(4-chlorophenyl)ethan-1-one (5c). Yield = 81%, mp = 101−106 °C, yellow solid, IR (KBr, v, cm^{-1}): 1721 (C=O), 3217 and 3456 (NH$_2$); ^{1}H NMR (400 MHz, DMSO-d_6): δ = 1.72 (s, 4H, 2CH$_2$), 2.29 (m, 2H, CH$_2$), 2.60 (s, 2H, CH$_2$), 5.56 (s, 1H, CH of pyran), 5.59 (s, 2H, COCH$_2$O), 5.77 (s, 2H, NH$_2$; D$_2$O exchangeable), 6.70 (d, J = 8.5 Hz, 1H, ArH), 6.81 (s, 1H, ArH), 7.14 (d, J = 8.5 Hz, 1H, ArH), 7.55 (t, J = 7.9 Hz, 1H, ArH), 7.64 (s, 1H, ArH), 7.66 (d, J = 8.0 Hz, 2H, ArH), 8.01 (s, 1H, ArH), 8.04 (d, J = 8.4 Hz, 2H, ArH), 8.27 (s, 1H, ArH); ^{13}C NMR (100 MHz, DMSO-d_6): 22.49, 22.69, 23.38, 32.42, 38.39, 70.65, 98.05, 102.86, 111.51, 112.88, 117.37, 121.91, 122.14, 129.45, 130.05, 130.29, 130.76, 133.31, 134.30, 139.27, 148.19, 151.76, 152.01, 153.41, 155.69, 158.17, 194.12; MS (EI) m/z (C$_{30}$H$_{24}$N$_3$O$_5$Cl): 543.95 (M$^+$ + 2, 6.48%), 542.58 (M$^+$ + 1, 12.92%), 541.80 (M$^+$, 44.50%), 50.90 (100%); HRMS (m/z): [M + H]$^+$ calcd for C$_{30}$H$_{24}$N$_3$O$_5$Cl: 542.1477; found: 542.14659; elemental analysis for C$_{30}$H$_{24}$N$_3$O$_5$Cl, calcd: C, 66.48; H, 4.46; N, 7.7S; found: C, 66.54; H, 4.33; N, 7.62.

5.1.4.4. Characterization of 2-[11-Amino-12-(3,4-dichlorophenyl)-7,9,10,12-tetrahydro-8H-chromeno[2, 3-b]-quinolin-3-yl]oxy-1-(4-chlorophenyl)ethan-1-one (5d). Yield = 94%, mp = 113−117 °C, yellow solid, IR (KBr, v, cm^{-1}): 1699 (C=O), 3367 and 3480 (NH$_2$); ^{1}H NMR (400 MHz, DMSO-d_6): δ = 1.72 (s, 4H, 2CH$_2$), 2.30 (m, 2H, CH$_2$), 2.59 (s, 2H, CH$_2$), 5.37 (s, 1H, CH of pyran), 5.59 (s, 2H, COCH$_2$O), 5.71 (s, 2H, NH$_2$; D$_2$O exchangeable), 6.70 (dd, J = 2.3, 8.5 Hz, 1H, ArH), 6.78 (d, J = 2.1 Hz, 1H, ArH), 7.12 (d, J = 8.5 Hz, 2H, ArH), 7.50 (d, J = 8.4 Hz, 1H, ArH), 7.66 (t, J = 7.5 Hz, 3H, ArH), 8.05 (d, J = 8.5 Hz, 2H, ArH); ^{13}C NMR (100 MHz, DMSO-d_6): 22.54, 22.75, 23.42, 32.52, 38.00, 70.74, 97.95, 102.84, 111.4S, 112.79, 117.32, 127.90, 129.44, 129.54, 129.97, 130.32, 131.30, 131.43, 133.43, 139.22, 147.13, 151.72, 151.92, 153.30, 155.62, 158.16, 194.07; HRMS (m/z): [M + H]$^+$ calcd for C$_{30}$H$_{23}$N$_2$O$_3$Cl$_3$: 565.0847; found: 565.08319; elemental analysis for C$_{30}$H$_{23}$N$_2$O$_3$Cl$_3$, calcd: C, 63.68; H, 4.10; N, 4.95; found: C, 63.60; H, 4.00; N, 4.85.

5.1.4.5. Characterization of 2-[11-Amino-12-(2-methoxyphenyl)-7,9,10,12-tetrahydro-8H-chromeno[2, 3-b]-quinolin-3-yl]oxy-1-(4-chlorophenyl)ethan-1-one (5e). Yield = 80%, mp = 105−110 °C, yellow solid; ^{1}H NMR (400 MHz, DMSO-d_6): δ = 1.70 (s, 4H, 2CH$_2$), 2.26 (m, 2H, CH$_2$), 2.57 (s, 2H, CH$_2$), 3.91 (s, 3H, OCH$_3$), 5.28 (s, 2H, NH$_2$; D$_2$O exchangeable), 5.48 (s, 1H, CH of pyran), 5.56 (s, 2H, COCH$_2$O), 6.63 (s, 1H, ArH), 6.82 (m, 2H, ArH), 7.03 (d, J = 7.6 Hz, 2H, ArH), 7.15 (s, 2H, ArH), 7.67 (s, 2H, ArH), 8.05 (d, J = 5.8 Hz, 2H, ArH); elemental analysis for C$_{31}$H$_{27}$N$_2$O$_4$Cl, calcd: C, 70.65; H, 5.16; N, 5.32; found: C, 70.51; H, 5.21; N, 5.45.

5.1.4.6. Characterization of 2-[11-Amino-12-(3-bromophenyl)-7,9,10,12-tetrahydro-8H-chromeno[2, 3-b]quinolin-3-yl]oxy-1-phenylethan-1-one (5f). Yield = 88%, mp = 102−107 °C, yellow solid, IR (KBr, v, cm^{-1}): 1701 (C=O), 3391 and 3483 (NH$_2$); ^{1}H NMR (400 MHz, DMSO-d_6): δ = 1.73 (s, 4H, 2CH$_2$), 2.30 (m, 2H, CH$_2$), 2.59 (s, 2H, CH$_2$), 5.34 (s, 1H, CH of pyran), 5.60 (s, 2H, COCH$_2$O), 5.68 (s, 2H, NH$_2$; D$_2$O exchangeable), 6.70 (d, J = 7.7 Hz, 1H, ArH), 6.77 (s, 1H, ArH), 7.11 (d, J = 8.4 Hz, 1H, ArH), 7.22 (s, 2H, ArH), 7.34 (s, 2H, ArH), 7.54 (s, 1H, ArH), 7.54 (t, J = 7.0, 1H, ArH), 7.59 (t, J = 7.3 Hz, 1H, ArH), 8.04 (d, J = 7.0 Hz, 2H, ArH); ^{13}C NMR (100 MHz, DMSO-d_6): 22.54, 22.76, 23.45, 32.58, 38.47, 70.70, 98.73, 102.87, 111.36, 112.82, 117.82, 122.12, 126.70, 128.36, 129.32, 129.78, 129.91, 130.20, 131.34, 134.30, 134.85, 148.90, 151.82, 151.87, 153.14, 155.75, 158.17, 195.05; elemental analysis for C$_{30}$H$_{25}$N$_2$O$_3$Br, calcd: C, 66.55; H, 4.65; N, 5.17; found: C, 66.60; H, 4.74; N, 5.23.

5.1.4.7. Characterization of 2-[11-Amino-12-(3-methoxyphenyl)-7,9,10,12-tetrahydro-8H-chromeno[2, 3-b]-quinolin-3-yl]oxy-1-phenylethan-1-one (5g). Yield = 74%, mp = 115−120 °C, yellow solid; ^{1}H NMR (400 MHz, DMSO-d_6): δ = 1.72 (s, 4H, 2CH$_2$), 2.29 (m, 2H, CH$_2$), 2.58 (s, 2H, CH$_2$), 3.70 (s, 3H, OCH$_3$), 5.25 (s, 1H, CH of pyran), 5.55 (s, 2H, NH$_2$; D$_2$O exchangeable), 5.58 (s, 2H, COCH$_2$O), 6.66 (m, 2H, ArH), 6.74 (m, 2H, ArH), 6.94 (s, 1H, ArH), 7.13 (m, 2H, ArH), 7.58 (t, J = 7.6 Hz, 2H, ArH), 7.71 (t, J = 7.3 Hz, 1H, ArH), 8.03 (d, J = 7.1 Hz, 2H, ArH); ^{13}C NMR (100 MHz, DMSO-d_6): 22.61, 22.84, 23.45, 32.56, 38.91, 55.25, 70.71, 98.72, 102.63, 111.09, 111.34, 112.57, 114.26, 118.29, 119.83, 128.36, 129.32, 129.90, 130.16, 134.31, 134.84, 147.72, 151.72, 151.87, 152.82, 155.75, 157.95, 159.66, 194.90; elemental analysis for C$_{31}$H$_{28}$N$_2$O$_4$, calcd: C, 75.59; H, 5.73; N, 5.69; found: C, 75.67; H, 5.81; N, 5.62.

5.1.4.8. Characterization of 2-[11-Amino-12-(3-nitrophenyl)-7,9,10,12-tetrahydro-8H-chromeno[2, 3-b]quinolin-3-yl]oxy-1-phenylethan-1-one (5h). Yield = 86%, mp = 105−110 °C, yellow solid; ^{1}H NMR (400 MHz, DMSO-d_6): δ = 1.72 (s, 4H, 2CH$_2$), 2.29 (m, 2H, CH$_2$), 2.59 (s, 2H, CH$_2$), 5.56 (s, 1H, CH of pyran), 5.61 (s, 2H, COCH$_2$O), 5.78 (s, 2H, NH$_2$; D$_2$O exchangeable), 6.70 (d, J = 8.5 Hz, 1H, ArH), 6.80 (s, 1H, ArH), 7.13 (d, J = 8.5 Hz, 1H, ArH), 7.57 (m, 3H, ArH), 7.65 (d, J = 7.6 Hz, 1H, ArH), 7.17 (t, J = 7.2 Hz, 1H, ArH), 8.03 (d, J = 7.2 Hz, 3H, ArH), 8.28 (s, 1H, ArH); ^{13}C NMR (100 MHz, DMSO-d_6): 22.55, 22.78, 23.46, 32.51, 38.40, 70.83, 98.15, 102.90, 111.63, 113.07, 117.38, 117.42, 121.79, 128.36, 129.33, 129.96, 130.74, 134.33, 134.38, 134.77, 148.15, 148.37, 151.90, 151.96, 153.34, 155.74, 158.24, 194.63; elemental analysis for C$_{30}$H$_{25}$N$_3$O$_5$, calcd: C, 70.99; H, 4.97; N, 8.28; found: C, 70.88; H, 4.87; N, 8.34.

5.1.4.9. Characterization of 2-[11-Amino-12-(3,4-dichlorophenyl)-7,9,10,12-tetrahydro-8H-chromeno[2, 3-b]-

quinolin-3-yl]oxy-1-phenylethan-1-one (5i)*. Yield = 90%, mp = 112−117 °C, yellow solid, IR (KBr, *v*, cm^{-1}): 1702 (C=O), 3227 and 3392 (NH$_2$); ^{1}H NMR (400 MHz, DMSO-d_6): δ = 1.72 (s, 4H, 2CH$_2$), 2.30 (m, 2H, CH$_2$), 2.59 (s, 2H, CH$_2$), 5.37 (s, 1H, CH of pyran), 5.61 (s, 2H, COCH$_2$O), 5.72 (s, 2H, NH$_2$; D$_2$O exchangeable), 6.70 (d, *J* = 8.4 Hz, 1H, ArH), 6.77 (d, *J* = 8.4 Hz, 1H, ArH), 7.13 (d, *J* = 8.5 Hz, 2H, ArH), 7.51 (d, *J* = 8.4 Hz, 1H, ArH), 7.59 (t, *J* = 7.6 Hz, 2H, ArH), 7.64 (s, 1H, ArH), 7.71 (t, *J* = 7.2 Hz, 1H, ArH), 8.04 (d, *J* = 7.5 Hz, 2H, ArH); ^{13}C NMR (100 MHz, DMSO-d_6): 22.56, 22.78, 23.44, 32.56, 38.01, 70.77, 97.98, 102.88, 111.44, 112.78, 117.28, 127.93, 128.36, 129.33, 129.44, 129.52, 129.94, 131.28, 131.43, 134.33, 134.80, 147.18, 151.76, 151.91, 153.28, 155.64, 158.26, 194.92; MS (EI) *m/z* (C$_{30}$H$_{24}$N$_2$O$_3$Cl$_2$): 534.39 (M$^+$ + 2, 5.76%), 533.12 (M$^+$ + 1, 19.14%), 531.74 (M$^+$, 11.40%), 57.08 (100%); elemental analysis for C$_{30}$H$_{24}$N$_2$O$_3$Cl$_2$, calcd: C, 67.80; H, 4.55; N, 5.27; found: C, 67.74; H, 4.68; N, 5.31.

5.1.4.10. Characterization of 2-[11-Amino-12-(2-methoxyphenyl)-7,9,10,12-tetrahydro-8H-chromeno[2, 3-b]-quinolin-3-yl]oxy-1-phenylethan-1-one (5j). Yield = 73%, mp = 107−112 °C, yellow solid, IR (KBr, *v*, cm^{-1}): 1695 (C=O), 3371 and 3461 (NH$_2$); ^{1}H NMR (400 MHz, DMSO-d_6): δ = 1.71 (s, 4H, 2CH$_2$), 2.27 (m, 2H, CH$_2$), 2.57 (s, 2H, CH$_2$), 3.92 (s, 3H, OCH$_3$), 5.28 (s, 2H, NH$_2$; D$_2$O exchangeable), 5.48 (s, 1H, CH of pyran), 5.58 (s, 2H, COCH$_2$O), 6.63 (dd, *J* = 2.4, 8.5 Hz, 1H, ArH), 6.73 (d, *J* = 2.4, 1H, ArH), 6.83 (t, *J* = 7.4 Hz, 1H, ArH), 6.91 (d, *J* = 6.6 Hz, 1H, ArH), 7.02 (m, 2H, ArH), 7.15 (t, *J* = 7.7 Hz, 1H, ArH), 7.59 (t, *J* = 7.7 Hz, 2H, ArH), 7.71 (t, *J* = 7.3 Hz, 1H, ArH), 8.04 (d, *J* = 7.4 Hz, 2H, ArH); ^{13}C NMR (100 MHz, DMSO-d_6): 22.59, 22.84, 23.35, 32.15, 32.52, 56.45, 70.75, 98.83, 102.43, 111.10, 111.97, 112.42, 117.77, 121.88, 128.28, 128.36, 129.32, 129.64, 130.00, 134.05, 134.31, 134.84, 151.59, 151.95, 152.67, 155.50, 155.66, 157.87, 194.97; HRMS (*m/z*): [M + H]$^+$ calcd for C$_{31}$H$_{28}$N$_2$O$_4$: 493.2122; found: 493.21148; elemental analysis for C$_{31}$H$_{28}$N$_2$O$_4$, calcd: C, 75.59; H, 5.73; N, 5.69; found: C, 75.65; H, 5.61; N, 5.82.

5.2. Biology. *5.2.1. In Vitro AChE and BuChE Inhibition Assay.* The anticholinesterase activity of target compounds was assessed *in vitro* against AChE by using the spectrophotometric method of Ellman[84] (K197-100, Bio Vision assay kit). A mixture of 5,5′-dithio-bis(2-nitrobenzoic acid) (DTNB, 160 μL), *h*AChE or *h*BuChE solution (50 μL), compound solution (10 μL), and buffer (50 μL) was preincubated for 10 min in a 96-well plate. Then, the substrate acetylthiocholine iodide or butyryl thiocholine iodide was added. In parallel, a blank containing all components without the enzyme was used in order to account for the nonenzymatic reaction. Changes in absorbance were measured at 412 nm for 5 min at 25 °C. The IC$_{50}$ values were determined graphically from the log concentration vs. % of inhibition curves. The percentage of relative inhibition was determined from the following equation (where EC is the enzyme control and S is the sample)

$$\% \text{ relative inhibition} = \frac{\text{slope of EC} - \text{slope of S}}{\text{slope of Ec}} \times 100$$

$$\% \text{ relative activity} = \frac{\text{slope of S}}{\text{slope of EC}} \times 100$$

5.2.2. β-Secretase Inhibition Assay. The β-secretase inhibition assay was carried out using the following procedure

by employing a convenient fluorescence method (K720-100, Bio Vision assay kit). The reaction mixture consisted of various concentrations of the test compound or DMSO (control), and certain amounts of the enzyme and an appropriate sodium acetate buffer were preincubated at 25 °C. Then, the substrate was added to initiate the reaction and incubated for 5−60 min at 37 °C. The fluorescence signal was recorded by a fluorescent plate reader with E_x/E_m = 345/500 nm. The slope can be calculated by dividing the net ΔRFU (=RFU$_2$−RFU$_1$) value by time Δt (=t_2−t_1). The % relative inhibition and % relative activity were calculated using the following equation (where the slope of EC is the slope of the enzyme control and the slope of S is the slope of the sample screen)

$$\% \text{ relative inhibition} = \frac{\text{slope of EC} - \text{slope of S}}{\text{slope of Ec}} \times 100$$

$$\% \text{ relative activity} = \frac{\text{slope of S}}{\text{slope of EC}} \times 100$$

5.2.3. MAO-B Inhibition Assay. The *in vitro* fluorometric method was used to evaluate the inhibition potency of the synthesized compounds on MAO-B (K797-100, Bio Vision assay kit). This assay is based on the fluorometric detection of H$_2$O$_2$, one of the byproducts generated during the oxidative deamination of the MAO substrate (Tyramine). The promising compounds were dissolved in a proper solvent and diluted with an assay buffer to 0.01−10 μM. For each well, 50 μL of an MAO-B enzyme solution was prepared (49 μL of MAO-B assay buffer and 1 μL of diluted MAO-B enzyme). 50 μL/well was added into wells containing the target compounds, inhibitor control, and enzyme control. Next, they were incubated for 10 min at 37 °C. Intended for MAO-B substrate solution preparation: each well contained 40 μL of the MAO-B substrate solution (37 μL of the MAO-B assay buffer, 1 μL of the MAO-B substrate, 1 μL of developer, and 1 μL of the OxiRed probe). Then, they were mixed well and 40 μL of the MAO-B substrate solution was added into each well. The fluorescence was measured kinetically at 37 °C for 10−40 min (E_x/E_m = 535/587 nm). Two points (T_1 and T_2) in the linear range of the plot were chosen to obtain the corresponding fluorescence values (RFU$_1$ and RFU$_2$). The slope was calculated for all samples, including the enzyme control (EC), by dividing the net ΔRFU (RFU$_2$−RFU$_1$) values by the time ΔT (T_2−T_1). The % relative inhibition was calculated as follows:

$$\% \text{ relative inhibition} = \frac{(\text{slope of EC} - \text{slope of S})}{\text{slope of Ec}} \times 100$$

5.2.4. Determination of the Inhibitory Potency on Aβ$_{1−42}$ Self-Aggregation. In order to investigate the self-mediated Aβ$_{1−42}$ aggregation, a thioflavin-T fluorescence assay was performed[85] using K570-100 (Bio Vision assay kit) as it included a dye that binds to the β sheets of an aggregated amyloid peptide, resulting in an intense fluorescent product (E_x/E_m: 440/490 nm). In the presence of an Aβ$_{1−42}$ ligand, this reaction is impeded/abolished, resulting in a decrease or total loss of fluorescence. The promising compounds were dissolved in DMSO and diluted with an Aβ$_{42}$ assay buffer. For sample screening (S) preparation, each well contained 50 μL of tested compounds, while for peptide control (PC) and solvent control (SC), each well contained 50 μL of an assay buffer or a solvent, respectively. Each well contained 2 μL of an Aβ$_{42}$

inhibitor control, and the volume was adjusted to 50 μL by an Aβ_{42} assay buffer for inhibitor control preparation. The Aβ_{42} peptide was diluted by adding 40 μL of Aβ_{42} peptide into 40 μL of an Aβ42 assay buffer. After that, 80 μL of diluted Aβ_{42} peptide was added to S, PC, SC, and inhibitor control wells. Later, 70 μL of the reaction mix composed of 68 μL of the assay buffer and 2 μL of the Aβ42 probe was added into each well containing S, PC, SC, and the inhibitor control. The plate was covered, shaken gently for 10 min, and incubated at 37 °C for 3 h. The fluorescence was measured at E_x/E_m = 440/490 nm; after setting the relative fluorescence units (RFUs) of the blank control as 100%, the relative activity was calculated with sample screening as follows:

$$\% \text{ relative activity} = \frac{\text{RFU of S}}{\text{RFU of PC}} \times 100$$

$$\% \text{ relative inhibition} = \frac{\text{RFU of PC} - \text{RFU of S}}{\text{RFU of S}} \times 100$$

5.2.5. Total Antioxidant Capacity Assay. The Total Antioxidant Capacity Assay Kit (Colorimetric) (ab65329) was used to measure the combination of antioxidants to the Cu^{2+} ion, which converted to Cu$^+$. The reduced Cu$^+$ ion is chelated with a colorimetric probe, giving a broad absorbance peak around OD 570 nm, proportional to the total antioxidant capacity. Each synthesized compound well contains 100 μL of the Cu^{2+} working solution. The plate was mixed and incubated at room temperature for 90 min on an Orbital shaker protected from light. The output was measured on a microplate reader at OD 570 nm. Calculations were completed by subtracting the mean absorbance value of the blank from all standard and sample readings, averaging the duplicate reading for each standard and sample and plotting the corrected absorbance values for each standard as a function of the final concentration of Trolox. Finally, we draw the best smooth curve through these points to construct the standard curve and then calculate the trendline equation based on the standard curve data. The concentration of Trolox (nmol/μL or mM) in the test samples is calculated as

$$\text{sample total antioxidant capacity} = \left(\frac{T_s}{S_v}\right)^* D$$

where T_s is the TAC amount in the sample well calculated from the standard curve (nmol), S_v is the sample volume added in the sample wells (μL), and D is the sample dilution factor.

5.2.6. In Vitro Neurotoxicity Assay. The cytotoxicity values of compounds **4c**, **4g**, **4n**, **5c**, **5d**, and **5i** were tested using the human neuroblastoma SH-SY5Y cell line. These cells were incubated according to the supplier's recommendations. Cells were seeded at 10,000 cells into each well of 96-well plates in DMEM/F-12 (Dulbecco's modified Eagle's medium) media containing 10% fetal bovine serum (FBS) and horse serum supplemented 1% penicillin antibiotic solution for 24 h. The MTT assay was carried out as previously reported.[86] The compound solution was tested between 0.39 and 100 μM concentrations in DMSO (1%). The IC$_{50}$ value was calculated by plotting a dose–response curve of % inhibition versus tested compound concentrations.

5.2.7. In Vitro Hepatotoxicity Assay. The cytotoxicity of active compounds **4c**, **4g**, **4n**, **5c**, **5d**, and **5i** on HepG2 cancer cells was evaluated by the MTT assay. The principle of this assay is the transformation of the yellow tetrazolium bromide

(MTT) to a purple formazan derivative by mitochondrial succinate dehydrogenase in viable cells.[87] Cell lines were cultured in the RPMI-1640 medium with 10% fetal bovine serum. The antibiotics added were 100 mg/mL streptomycin and 100 units/mL penicillin at 37 °C in a 5% CO$_2$ incubator. The cell lines were planted in a 96-well plate at a density of 1.0 10^4 cells/well at 37 °C for 48 h under 5% CO$_2$. After incubation, the cells were handled with several concentrations of the synthesized compounds and incubated for 24 h. After that, 20 μL of MTT solution at 5 mg/mL was included and incubated for 4 h. Dimethyl sulfoxide (DMSO) in a volume of 100 μL is supplemented into each well to dissolve the purple formazan made. The absorbance was measured at a wavelength of 570 nm using a plate reader (EXL 800 USA), and IC$_{50}$ values were determined.

5.2.8. Metal Chelation Assay. The chelating studies were achieved with a UV–visible Shimadzu spectrophotometer. The UV absorption spectra of the tested compounds alone or in the presence of CuSO$_4$, ZnSO$_4$, and FeSO$_4$ were recorded in ethanol with the wavelength ranging from 200 to 600 nm after incubating for 30 min at room temperature. The final concentrations of the tested compound and metals were 30 μM. Numerical subtraction of the spectra of the metal alone and the compound alone from the spectra of the mixture gave the difference in the UV–vis spectra due to complex formation.[65]

5.3. Docking Study. *5.3.1. Protein Preparation.* The crystal structures of AChE, BuChE, BACE-1, MAO-B, and amyloid Aβ_{1-42} with PDB IDs 4BDT, 4BDS, 2ZJM, 2V5Z, and 6SZF, respectively, were retrieved from the protein databank (www.rcsb.org). All of the crystal structures were organized individually by eliminating the current ligands and water molecules, although lost hydrogen atoms were supplemented *via* the Autodock program.[68,69] Subsequently, nonpolar hydrogens were combined, whereas the polar hydrogen was added to each enzyme. The process was recurrent for each protein and then saved into the dockable pdbqt format in preparation for molecular docking.

5.3.2. Ligand Preparation. The compounds were transformed into the Pdb chemical format using Discovery Studio Visualizer, BIOVIA, 2021. Polar hydrogens were added while nonpolar hydrogens were combined with the carbons, and the internal degrees of freedom and torsions were set using Autodock. The protein and ligand molecules were thereafter transformed to the dockable pdbqt format using Autodock tools.[68,69]

5.3.3. Molecular Docking. The docking of the ligands to various target proteins and evaluation of binding affinities was determined *via* Autodock using the Pdbqt format of the receptors, as well as those of the ligands, and the software was run. The binding affinities of compounds for the protein targets were recorded. The compounds were then classified by their affinity scores. For comparison of in silico performance, the molecular interactions between the receptors and compounds with a binding affinity equal to or greater than standard inhibitors were viewed with Discovery Studio Visualizer, BIOVIA, 2021.

■ ASSOCIATED CONTENT

ⓈI Supporting Information

The Supporting Information is available free of charge at https://pubs.acs.org/doi/10.1021/acsomega.3c02051.

^{1}H NMR and ^{13}C NMR of all synthesized compounds, MS and HRMS of selected compounds, and the biological data for the experimental section (PDF)

■ AUTHOR INFORMATION

Corresponding Author

Walaa M. El Husseiny − *Department of Pharmaceutical Organic Chemistry, Faculty of Pharmacy, Mansoura University, Mansoura 35516, Egypt;* ● orcid.org/0000-0002-0261-8264; Email: walaaelhusseiny@yahoo.com

Authors

Salma Fares − *Department of Pharmaceutical Organic Chemistry, Faculty of Pharmacy, Mansoura University, Mansoura 35516, Egypt; Department of Pharmaceutical Chemistry, Delta University For science and Technology, Gamasa 11152, Egypt*

Khalid B. Selim − *Department of Pharmaceutical Organic Chemistry, Faculty of Pharmacy, Mansoura University, Mansoura 35516, Egypt*

Mohammed A. M. Massoud − *Department of Pharmaceutical Organic Chemistry, Faculty of Pharmacy, Mansoura University, Mansoura 35516, Egypt*

Complete contact information is available at:
https://pubs.acs.org/10.1021/acsomega.3c02051

Notes
The authors declare no competing financial interest.

■ ACKNOWLEDGMENTS

■ REFERENCES

(1) Panek, D.; Wieckowska, A.; Jonczyk, J.; Godyn, J.; Bajda, M.; Wichur, T.; Pasieka, A.; Knez, D.; Pislar, A.; Korabecny, J.; Soukup, O.; Sepsova, V.; Sabate, R.; Kos, J.; Gobec, S.; Malawska, B. Design, Synthesis, and Biological Evaluation of 1-Benzylamino-2-hydroxyalkyl Derivatives as New Potential Disease-Modifying Multifunctional Anti-Alzheimer's Agents. *ACS Chem. Neurosci.* **2018**, *9*, 1074−1094.

(2) Mishra, P.; Kumar, A.; Panda, G. Anti-cholinesterase hybrids as multi-target-directed ligands against Alzheimer's disease (1998-2018). *Bioorg. Med. Chem.* **2019**, *27*, 895−930.

(3) Silman, I.; Sussman, J.-L. Acetylcholinesterase: 'classical' and 'non-classical' functions and pharmacology. *Curr. Opin. Pharmacol.* **2005**, *5*, 293−302.

(4) Suh, Y.-H.; Checler, F. Amyloid precursor protein, presenilins, and α-synuclein: molecular pathogenesis and pharmacological applications in Alzheimer's disease. *Pharmacol. Rev.* **2002**, *54*, 469−525.

(5) Okuda, M.; Hijikuro, I.; Fujita, Y.; Teruya, T.; Kawakami, H.; Takahashi, T.; Sugimoto, H. Design and synthesis of curcumin derivatives as tau and amyloid beta dual aggregation inhibitors. *Bioorg. Med. Chem. Lett.* **2016**, *26*, 5024−5028.

(6) Praticò, D. Oxidative stress hypothesis in Alzheimer's disease: a reappraisal. *Trends Pharmacol. Sci.* **2008**, *29*, 609−615.

(7) Kinney, J.-W.; Bemiller, S.-M.; Murtishaw, A.-S.; Leisgang, A.-M.; Salazar, A.-M.; Lamb, B.-T. Inflammation as a central mechanism in Alzheimer's disease. *Alzheimers Dement.* **2018**, *4*, 575−590.

(8) González-Domínguez, R.; García-Barrera, T.; Gómez-Ariza, J.-L. Homeostasis of metals in the progression of Alzheimer's disease. *BioMetals* **2014**, *27*, 539−549.

(9) Yan, R.; Vassar, R. Targeting the β secretase BACE1 for Alzheimer's disease therapy. *Lancet Neurol.* **2014**, *13*, 319−329.

(10) Rosini, M.; Simoni, E.; Caporaso, R.; Minarini, A. Multitarget strategies in Alzheimer's disease: benefits and challenges on the road to therapeutics. *Future Med. Chem.* **2016**, *8*, 697−711.

(11) Klafki, H.-W.; Staufenbiel, M.; Kornhuber, J.; Wiltfang, J. Therapeutic approaches to Alzheimer's disease. *Brain* **2006**, *129*, 2840−2855.

(12) Bartus, R. T.; Dean, R. L.; Pontecorvo, M. J.; Flicker, C. The cholinergic hypothesis: a historical overview, current perspective, and future directions. *Ann. N. Y. Acad. Sci.* **1985**, *444*, 332−358.

(13) Ali, R.; Gupta, G.-D.; Chawla, P.-A. Aducanumab: A new hope in Alzheimer's disease. *Health Sci. Rev.* **2022**, *4*, No. 100039.

(14) Jiang, N.; Huang, Q.; Liu, J.; Liang, N.; Li, Q.; Li, Q.; Xie, S.-S. Design, synthesis and biological evaluation of new coumarin-dithiocarbamate hybrids as multifunctional agents for the treatment of Alzheimer's disease. *Eur. J. Med. Chem.* **2018**, *146*, 287−298.

(15) Bartolini, M.; Bertucci, C.; Cavrini, V.; Andrisano, V. β-Amyloid aggregation induced by human acetylcholinesterase: inhibition studies. *Biochem. Pharmacol.* **2003**, *65*, 407−416.

(16) Shidore, M.; Machhi, J.; Shingala, K.; Murumkar, P.; Sharma, M. K.; Agrawal, N.; Tripathi, A.; Parikh, Z.; Pillai, P.; Yadav, M.-R. Benzylpiperidine-linked diarylthiazoles as potential anti-Alzheimer's agents: synthesis and biological evaluation. *J. Med. Chem.* **2016**, *59*, 5823−5846.

(17) Ismaili, L.; Refouvelet, B.; Benchekroun, M.; Brogi, S.; Brindisi, M.; Gemma, S.; Campiani, G.; Filipic, S.; Agbaba, D.; Esteban, G.; et al. Multitarget compounds bearing tacrine-and donepezil-like structural and functional motifs for the potential treatment of Alzheimer's disease. *Prog. Neurobiol.* **2017**, *151*, 4−34.

(18) Viayna, E.; Sola, I.; Bartolini, M.; De Simone, A.; Tapia-Rojas, C.; Serrano, F.-G.; Sabaté, R.; Juárez-Jiménez, J.; Pérez, B.; Luque, F.-J.; Andrisano, V.; Clos, M.-V.; Inestrosa, N.-C.; Muñoz-Torrero, D. Synthesis and Multitarget Biological Profiling of a Novel Family of Rhein Derivatives As Disease-Modifying Anti-Alzheimer Agents. *J. Med. Chem.* **2014**, *57*, 2549−2567.

(19) Shi, X.-L.; Wu, J.-D.; Liu, P.; Liu, Z.-P. Synthesis and evaluation of novel GSK-3β inhibitors as multifunctional agents against Alzheimer's disease. *Eur. J. Med. Chem.* **2019**, *167*, 211−225.

(20) Sinha, S.; Lieberburg, I. Cellular mechanisms of β-amyloid production and secretion. *Proc. Natl. Acad. Sci. U.S.A.* **1999**, *96*, 11049−11053.

(21) Giacobini, E.; Gold, G. Alzheimer disease therapy moving from amyloid-β to tau. *Nat. Rev. Neurol.* **2013**, *9*, 677−686.

(22) Tatarnikova, O.; Orlov, M.; Bobkova, N. Beta-amyloid and tau-protein: structure, interaction, and prion-like properties. *Biochemistry* **2015**, *80*, 1800−1819.

(23) Zatta, P.; Drago, D.; Bolognin, S.; Sensi, S.-L. Alzheimer's disease, metal ions and metal homeostatic therapy. *Trends Pharmacol. Sci.* **2009**, *30*, 346−355.

(24) Ha, C.; Ryu, J.; Park, C.-B. Metal ions differentially influence the aggregation and deposition of Alzheimer's β-amyloid on a solid template. *Biochemistry* **2007**, *46*, 6118−6125.

(25) Kozlowski, H.; Luczkowski, M.; Remelli, M.; Valensin, D. Copper, zinc and iron in neurodegenerative diseases (Alzheimer's, Parkinson's and prion diseases). *Coord. Chem. Rev.* **2012**, *256*, 2129−2141.

(26) Cacabelos, R.; Torrellas, C.; Carrera, I.; Cacabelos, P.; Corzo, L.; Fernandez-Novoa, L.; Tellado, I.; Carril, J.; Aliev, G. Novel therapeutic strategies for dementia. *CNS Neurol. Disord.: Drug Targets* **2016**, *15*, 41−241.

(27) Bonham, L.-W.; Desikan, R.-S.; Yokoyama, J.-S. The relationship between complement factor C3, APOE ε4, amyloid and tau in Alzheimer's disease. *Acta Neuropathol. Commun.* **2016**, *4*, No. 1355.

(28) Edmondson, D. E.; Mattevi, A.; Binda, C.; Li, M.; Hubalek, F. Structure and mechanism of monoamine oxidase. *Curr. Med. Chem.* **2004**, *11*, 1983−1993.

(29) Grimsby, J.; Lan, N.-C.; Neve, R.; Chen, K.; Shih, J.-C. Tissue distribution of human monoamine oxidase A and B Mrna. *J. Neurochem.* **1990**, *55*, 1166−1169.

(30) Carradori, S.; Silvestri, R. New frontiers in selective human MAO-B inhibitors: miniperspective. *J. Med. Chem.* **2015**, *58*, 6717−6732.

(31) He, Q.; Liu, J.; Lan, J.-S.; Ding, J.; Sun, Y.; Fang, Y.; Jiang, N.; Yang, Z.; Sun, L.; Jin, Y.; Xie, S.-S. Coumarin-dithiocarbamate hybrids as novel multitarget AChE and MAO-B inhibitors against Alzheimer's disease: Design, synthesis and biological evaluation. *Bioorg. Chem.* **2018**, *81*, 512−528.

(32) Schedin-Weiss, S.; Inoue, M.; Hromadkova, L.; Teranishi, Y.; Yamamoto, N.-G.; Wiehager, B.; Bogdanovic, N.; Winblad, B.; Sandebring-Matton, A.; Frykman, S. Monoamine oxidase B is elevated in Alzheimer disease neurons, is associated with γ-secretase and regulates neuronal amyloid β-peptide levels. *Alzheimer's Res. Ther.* **2017**, *9*, 1−19.

(33) Song, M.-S.; Matveychuk, D.; MacKenzie, E.-M.; Duchcherer, M.; Mousseau, D.-D.; Baker, G.-B. An update on amine oxidase inhibitors: Multifaceted drugs. *Prog. Neuro-Psychopharmacol. Biol. Psychiatry* **2013**, *44*, 118−124.

(34) Riederer, P. Monoamine Oxidase-B Inhibition in Alzheimer's Disease. *NeuroToxicology.* **2004**, *25*, 271−277.

(35) Watkins, P.-B.; Zimmerman, H.-J.; Knapp, M.-J.; Gracon, S.-I.; Lewis, K.-W. Hepatotoxic effects of tacrine administration in patients with Alzheimer's disease. *J. Am. Med. Assoc.* **1994**, *271*, 992−998.

(36) Monte-Millán, M. d.; García-Palomero, E.; Valenzuela, R.; Usán, P.; de Austria, C.; Muñoz-Ruiz, P.; Rubio, L.; Dorronsoro, I.; Martínez, A.; Medina, M. Dual binding site acetylcholinesterase inhibitors: potential new disease-modifying agents for AD. *J. Mol. Neurosci.* **2006**, *30*, 85−88.

(37) Romero, A.; Cacabelos, R.; Oset-Gasque, M.-J.; Samadi, A.; Marco-Contelles, J. Novel tacrine-related drugs as potential candidates for the treatment of Alzheimer's disease. *Bioorg. Med. Chem. Lett.* **2013**, *23*, 1916−1922.

(38) Costa, M.; Dias, T. A.; Brito, A.; Proenca, F. Biological importance of structurally diversified chromenes. *Eur. J. Med. Chem.* **2016**, *123*, 487−507.

(39) Yusufzai, S.-K.; Khan, M.-S.; Sulaiman, O.; Osman, H.; Lamjin, D.-N. Molecular docking studies of coumarin hybrids as potential acetylcholinesterase, butyrylcholinesterase, monoamine oxidase A/B and beta-amyloid inhibitors for Alzheimer's disease. *Chem. Cent. J.* **2018**, *12*, 128.

(40) Piazzi, L.; Rampa, A.; Bisi, A.; Gobbi, S.; Belluti, F.; Cavalli, A.; Bartolini, M.; Andrisano, V.; Valenti, P.; Recanatini, M. 3-(4-{[Benzyl (methyl) amino] methyl} phenyl)-6, 7-dimethoxy-2 H-2-chromenone (AP2238) Inhibits Both Acetylcholinesterase and Acetylcholinesterase-Induced β-Amyloid Aggregation: A Dual Function Lead for Alzheimer's Disease Therapy. *J. Med. Chem.* **2003**, *46*, 2279−2282.

(41) Yun, Y.; Miao, Y.; Sun, X.; Sun, J.; Wang, X. Synthesis and biological evaluation of 2-arylbenzofuran derivatives as potential anti-Alzheimer's disease agents. *J. Enzyme Inhib. Med. Chem.* **2021**, *36*, 1346−1356.

(42) Xie, S.-S.; Wang, X.; Jiang, N.; Yu, W.; Wang, K.-D.; Lan, J. S.; Li, Z.-R.; Kong, L.-Y. Multi-target tacrine-coumarin hybrids: cholinesterase and monoamine oxidase B inhibition properties against Alzheimer's disease. *Eur. J. Med. Chem.* **2015**, *95*, 53−165.

(43) Socier, L.; Rosselin, M.; Gomez Giraldo, A.-M.; Chantemargue, B.; Di Meo, F.; Trouillas, P.; Durand, G.; Morandat, S. Nitrone-Trolox conjugate as an inhibitor of lipid oxidation: Towards synergistic antioxidant effects, Biochim. Biophys. *Biochim. Biophys. Acta, Biomembr.* **2019**, *1861*, 1489−1501.

(44) Fernandez-Bachiller, M. -I.; Perez, C.; Monjas, L.; Rademann, J.; Rodriguez-Franco, M.-I. New tacrine-4-oxo-4H-chromene hybrids as multifunctional agents for the treatment of Alzheimer's disease, with cholinergic, antioxidant, and beta-amyloid-reducing properties. *J. Med. Chem.* **2012**, *55*, 1303−1317.

(45) Xie, S.-S.; Wang, X.-B.; Li, J.-Y.; Yang, L.; Kong, L.-Y. Design, synthesis and evaluation of novel tacrine-coumarin hybrids as

multifunctional cholinesterase inhibitors against Alzheimer's disease. *Eur. J. Med. Chem.* **2013**, *64*, 540−553.

(46) Xie, S.-S.; Wang, X.; Jiang, N.; Yu, W.; Wang, K.-D.; Lan, J.-S.; Li, Z. R.; Kong, L. Y. Multi-target tacrine-coumarin hybrids: cholinesterase and monoamine oxidase B inhibition properties against Alzheimer's disease. *Eur. J. Med. Chem.* **2015**, *95*, 153−165.

(47) Marco-Contelles, J.; Leon, R.; de los Rios, C.; Garcia, A. G.; Lopez, M. G.; Villarroya, M. New multipotent tetracyclic tacrines with neuroprotective activity. *Bioorg. Med. Chem.* **2006**, *14*, 8176−8185.

(48) Kidwai, M.; Saxena, S.; Khan, M. K.; Thukral, S. S. Aqua mediated synthesis of substituted 2-amino-4H-chromenes and in vitro study as antibacterial agents. *Bioorg. Med. Chem. Lett.* **2005**, *15*, 4295−4298.

(49) Marco-Contelles, J.; Pérez-Mayoral, E.; Samadi, A.; Carreiras, M.; Soriano, E. Recent Advances in the Friedländer Reaction. *Chem. Rev.* **2009**, *109*, 2652−2671.

(50) El-Gamal, M.-I.; Semreen, M.-H.; Foster, P.-A.; Potter, B.-V. Design, synthesis, and biological evaluation of new arylamide derivatives possessing sulfonate or sulfamate moieties as steroid sulfatase enzyme inhibitors. *Bioorg. Med. Chem.* **2016**, *24*, 2762−2767.

(51) El-Gamal, M.-I.; Zaraei, S.-O.; Foster, P.-A.; Anbar, H.-S.; El-Gamal, R.; El-Awady, R.; Potter, B.-V.-L. A new series of aryl sulfamate derivatives: Design, synthesis, and biological evaluation. *Bioorg. Med. Chem.* **2022**, *28*, No. 115406.

(52) Wang, Z.; Gu, J.; Jing, H.; Liang, Y. Novel one-pot synthesis of 3-phenylnaphtho [2, 3-b] furan and 3-phenylbenzofurans under microwave irradiation and solvent-free conditions. *Synth. Commun.* **2009**, *39*, 4079−4087.

(53) Perry, E. Acetylcholine and Alzheimer's disease. *Br. J. Psychiatry* **1988**, *152*, 737−740.

(54) Ellman, G.-L.; Courtney, K.-D.; Andres, V.; Featherstone, R.-M. A new and rapid colorimetric determination of acetylcholinesterase activity. *Biochem. Pharmacol.* **1961**, *7*, 88−95.

(55) Ma, L.; Yang, Z.; Li, C.; Zhu, Z.; Shen, X.; Hu, L. Design, synthesis and SAR study of hydroxychalcone inhibitors of human β-secretase (BACE1). *J. Enzyme Inhib. Med. Chem.* **2011**, *26*, 643−648.

(56) Choubey, P.-K.; Tripathi, A.; Tripathi, M.-K.; Seth, A.; Shrivastava, S.-K. Design, synthesis, and evaluation of N-benzylpyrrolidine and 1,3,4-oxadiazole as multitargeted hybrids for the treatment of Alzheimer's disease. *Bioorg. Chem.* **2021**, *111*, No. 104922.

(57) Xue, C.; Lin, T. Y.; Chang, D.; Guo, Z. Thioflavin T as an amyloid dye: fibril quantification, optimal concentration and effect on aggregation. *R. Soc. Open Sci.* **2017**, *4*, No. 160696.

(58) Ono, K.; Hasegawa, K.; Naiki, H.; Yamada, M. Curcumin has potent anti-amyloidogenic effects for Alzheimer's β-amyloid fibrils in vitro. *J. Neurosci. Res.* **2004**, *75*, 742−750.

(59) Christen, Y. Oxidative stress and Alzheimer disease. *Am. J. Clin. Nutr.* **2000**, *71*, 621S−629S.

(60) Huang, S.-W.; Hopia, A.; Schwarz, K.; Frankel, E. N.; German, J.-B. Antioxidant activity of α-tocopherol and trolox in different lipid substrates: bulk oils vs oil-in-water emulsions. *J. Agric. Food Chem.* **1996**, *44*, 444−452.

(61) Angius, F.; Floris, A. Liposomes and MTT cell viability assay: an incompatible affair. *Toxicol. In Vitro* **2015**, *29*, 314−319.

(62) Colovic, M. B.; Krstic, D.-Z.; Lazarevic-Pasti, T.-D.; Bondzic, A.-M.; Vasic, V.-M. Acetylcholinesterase inhibitors: pharmacology and toxicology. *Curr. Neuropharmacol.* **2013**, *11*, 315−335.

(63) Kepp, K.-P. Bioinorganic Chemistry of Alzheimer's Disease. *Chem. Rev.* **2012**, *112*, 5193−5239.

(64) Lee, H.-J.; Korshavn, K.-J.; Kochi, A.; Derrick, J.-S.; Lim, M.-H. Cholesterol and metal ions in Alzheimer's disease. *Chem. Soc. Rev.* **2014**, *43*, 6672−6682.

(65) Umar, T.; Shalini, S.; Raza, M.-K.; Gusain, S.; Kumar, J.; Seth, P.; Tiwari, M.; Hoda, N.-A. A multifunctional therapeutic approach: Synthesis, biological evaluation, crystal structure and molecular docking of diversified 1H-pyrazolo[3,4-b]pyridine derivatives against Alzheimer's disease. *Eur. J. Med. Chem.* **2019**, *175*, 2−19.

(66) Da Silva, M. L. B.; Ruiz-Aguilar, G.-M.; Alvarez, P.-J. Enhanced anaerobic biodegradation of BTEX-ethanol mixtures in aquifer

columns amended with sulfate, chelated ferric iron or nitrate. *Biodegradation* **2005**, *16*, 105−114.

(67) Blood−Brain Barrier (BBB) Prediction Server, 2022. http://www.cbligand.org/BBB/index.php.

(68) Goodsell, D. S.; Morris, G. M.; Olson, A. J. Automated docking of flexible ligands: applications of AutoDock. *J. Mol. Recognit.* **1996**, *9*, 1−5.

(69) Huey, R.; Morris, G. M.; Forli, S. *Using AutoDock 4 and AutoDock Vina with AutoDockTools: A Tutorial*; The Scripps Research Institute Molecular Graphics Laboratory, 2012; Vol. *10550*, p 92037.

(70) Johnson, G.; Moore, S.-W. The Peripheral Anionic Site of Acetylcholinesterase: Structure, Functions and Potential Role in Rational Drug Design. *Curr. Pharm. Des.* **2006**, *12*, 217−225.

(71) De Ferrari, G.-V.; Canales, M.-A.; Shin, I.; Weiner, L.-M.; Silman, I.; Inestrosa, N.-C. A Structural Motif of Acetylcholinesterase That Promotes Amyloid β-Peptide Fibril Formation. *Biochemistry* **2001**, *40*, 10447−10457.

(72) Çokuğraş, A. N. Butyrylcholinesterase: structure and physiological importance. *Turk. J. Biochem.* **2003**, *28*, 54−61.

(73) Nachon, F.; Carletti, E.; Ronco, C.; Trovaslet, M.; Nicolet, Y.; Jean, L.; Renard, P. Y. Crystal structures of human cholinesterases in complex with huprine W and tacrine: elements of specificity for anti-Alzheimer's drugs targeting acetyl- and butyryl-cholinesterase. *Biochem. J.* **2013**, *453*, 393−399.

(74) Rueeger, H.; Lueoend, R.; Rogel, O.; Rondeau, J.-M.; Möbitz, H.; Machauer, R.; Jacobson, L.; Staufenbiel, M.; Desrayaud, S.; Neumann, U. Discovery of Cyclic Sulfone Hydroxyethylamines as Potent and Selective β-Site APP-Cleaving Enzyme 1 (BACE1) Inhibitors: Structure-Based Design and in Vivo Reduction of Amyloid β-Peptides. *J. Med. Chem.* **2012**, *55*, 3364−3386.

(75) Wang, Q.; Yu, X.; Li, L.; Zheng, J. Inhibition of amyloid-β aggregation in Alzheimer's disease. *Curr. Pharm. Des.* **2014**, *20*, 1223−1243.

(76) Sciarretta, K.-L.; Gordon, D. J.; Petkova, A.-T.; Tycko, R.; Meredith, S.-C. Aβ40-Lactam(D23/K28) Models a Conformation Highly Favorable for Nucleation of Amyloid. *Biochemistry* **2005**, *44*, 6003−6014.

(77) Geha, R.-M.; Chen, K.; Wouters, J.; Ooms, F.; Shih, J.-C. Analysis of conserved active site residues in monoamine oxidase A and B and their three-dimensional molecular modeling. *J. Biol. Chem.* **2002**, *277*, 17209−17216.

(78) Ferrazzano, L.; Viola, A.; Lonati, E.; Bulbarelli, A.; Musumeci, R.; Cocuzza, C.; Lombardo, M.; Tolomelli, A. New isoxazolidinone and 3,4-dehydro-β-proline derivatives as antibacterial agents and MAO-inhibitors: A complex balance between two activities. *Eur. J. Med. Chem.* **2016**, *124*, 906−919.

(79) De Colibus, L.; Li, M.; Binda, C.; Lustig, A.; Edmondson, D.-E. Mattevi, Three-dimensional structure of human monoamine oxidase A (MAO A): relation to the structures of rat MAO A and human MAO B. *Proc. Natl. Acad. Sci.* **2005**, *102*, 12684−12689.

(80) Binda, C.; Hubálek, F.; Li, M.; Edmondson, D.-E.; Mattevi, A. Crystal structure of human monoamine oxidase B, a drug target enzyme monotopically inserted into the mitochondrial outer membrane. *FEBS Lett.* **2004**, *564*, 225−228.

(81) Geha, R. M.; Rebrin, I.; Chen, K.; Shih, J.-C. Substrate and inhibitor specificities for human monoamine oxidase A and B are influenced by a single amino acid. *J. Biol. Chem.* **2001**, *276*, 9877−9882.

(82) Milczek, E. M.; Binda, C.; Rovida, S.; Mattevi, A.; Edmondson, D. E. The 'gating'residues Ile199 and Tyr326 in human monoamine oxidase B function in substrate and inhibitor recognition. *FEBS J.* **2011**, *278*, 4860−4869.

(83) Elkamhawy, A.; Paik, S.; Kim, H.-J.; Park, J.-H.; Londhe, A.-M.; Lee, K.; Pae, A.-N.; Park, K.-D.; Roh, E.-J. Discovery of N-(1-(3-fluorobenzoyl)-1 H-indol-5-yl) pyrazine-2-carboxamide: a novel, selective, and competitive indole-based lead inhibitor for human monoamine oxidase B. *J. Enzyme Inhib. Med. Chem.* **2020**, *35*, 1568−1580.

(84) Ellman, G.-L.; Courtney, K.-D.; Andres, V., Jr; Featherstone, R.-M. A new and rapid colorimetric determination of acetylcholinesterase activity. *Biochem. Pharmacol.* **1961**, *7*, 88−95.

(85) Bartolini, M.; Bertucci, C.; Bolognesi, M.-L.; Cavalli, A.; Melchiorre, C.; Andrisano, V. Insight Into the Kinetic of Amyloid β(1−42) Peptide Self-Aggregation: Elucidation of Inhibitors' Mechanism of Action. *Chem. Biochem.* **2007**, *8*, 2152−2161.

(86) Osmaniye, D.; Levent, S.; Karaduman, A.-B.; Ilgın, S.; Özkay, Y.; Kaplancıklı, Z. A. Synthesis of New Benzothiazole Acylhydrazones as Anticancer Agents. *Molecules* **2018**, *23*, 1054.

(87) Sylvester, P. W. Optimization of the Tetrazolium Dye (MTT) Colorimetric Assay for Cellular Growth and Viability. In *Drug Design and Discovery: Methods and Protocols*; Humana Press, 2011; Vol. *716*, pp 157−168.